Article

Molecular Cell

Structural Basis for the Action of an All-Purpose Transcription Anti-termination Factor

Graphical Abstract

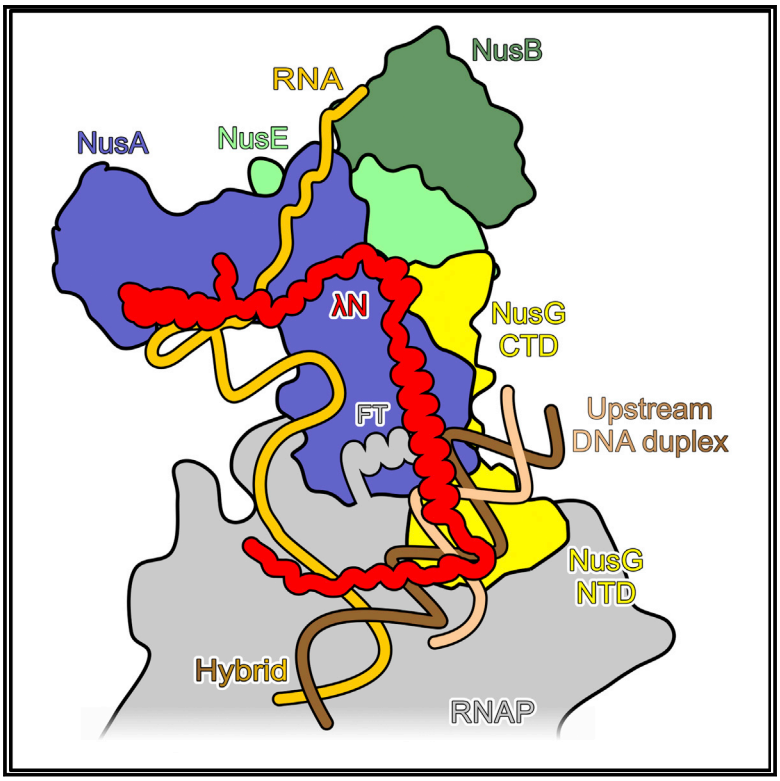

Authors

Ferdinand Krupp, Nelly Said, Yong-Heng Huang, ..., Thorsten Mielke, Christian M.T. Spahn, Markus C. Wahl

Correspondence

christian.spahn@charite.de (C.M.T.S.), markus.wahl@fu-berlin.de (M.C.W.)

In Brief

The cryo-EM structure of a λN-dependent transcription anti-termination complex shows how λN repositions the Nus factors on RNA polymerase, preventing NusA-mediated stabilization of RNA hairpins in the exit tunnel and overriding ρ-supporting functions of NusG. The C-terminal region of N traverses the hybrid cavity, stabilizing polymerase in a processive conformation.

Highlights

- λN positions NusA and NusE to destabilize RNA hairpins and NusG-ρ interaction
- λN remodels the flap tip and the RNA exit tunnel to fend off regulatory hairpins
- λN stabilizes elongating RNAP and undermines RNA exit-tunnel-active site signaling
- λN collaborates with NusG in stabilizing upstream DNA to prevent RNAP backtracking

Krupp et al., 2019, Molecular Cell *74*, 1–15
April 4, 2019
https://doi.org/10.1016/j.molcel.2019.01.016

CellPress

Please cite this article in press as: Krupp et al., Structural Basis for the Action of an All-Purpose Transcription Anti-termination Factor, Molecular Cell (2019), https://doi.org/10.1016/j.molcel.2019.01.016

Molecular Cell
Article

Structural Basis for the Action of an All-Purpose Transcription Anti-termination Factor

Ferdinand Krupp,[1,5] Nelly Said,[2,5] Yong-Heng Huang,[2,5] Bernhard Loll,[2] Jörg Bürger,[1,3] Thorsten Mielke,[3] Christian M.T. Spahn,[1,*] and Markus C. Wahl[2,4,6,*]
[1]Medizinische Physik und Biophysik, Charité – Universitätsmedizin Berlin, Charitéplatz 1, 10117 Berlin, Germany
[2]Freie Universität Berlin, Laboratory of Structural Biochemistry, Takustraβe 6, 14195 Berlin, Germany
[3]Max-Planck-Institut für Molekulare Genetik, Microscopy and Cryo-Electron Microscopy Group, Ihnestraße 63-73, 14195 Berlin, Germany
[4]Helmholtz-Zentrum Berlin für Materialien und Energie, Macromolecular Crystallography, Albert-Einstein-Straße 15, 12489 Berlin, Germany
[5]These authors contributed equally
[6]Lead Contact
*Correspondence: christian.spahn@charite.de (C.M.T.S.), markus.wahl@fu-berlin.de (M.C.W.)
https://doi.org/10.1016/j.molcel.2019.01.016

SUMMARY

Bacteriophage λN protein, a model anti-termination factor, binds nascent RNA and host Nus factors, rendering RNA polymerase resistant to all pause and termination signals. A 3.7-Å-resolution cryo-electron microscopy structure and structure-informed functional analyses reveal a multi-pronged strategy by which the intrinsically unstructured λN directly modifies RNA polymerase interactions with the nucleic acids and subverts essential functions of NusA, NusE, and NusG to reprogram the transcriptional apparatus. λN repositions NusA and remodels the β subunit flap tip, which likely precludes folding of pause or termination RNA hairpins in the exit tunnel and disrupts termination-supporting interactions of the α subunit C-terminal domains. λN invades and traverses the RNA polymerase hybrid cavity, likely stabilizing the hybrid and impeding pause- or termination-related conformational changes of polymerase. λN also lines upstream DNA, seemingly reinforcing anti-backtracking and anti-swiveling by NusG. Moreover, λN-repositioned NusA and NusE sequester the NusG C-terminal domain, counteracting ρ-dependent termination. Other anti-terminators likely utilize similar mechanisms to enable processive transcription.

INTRODUCTION

Bacteria transcribe their genomes with the help of a multi-subunit RNA polymerase (RNAP), which comprises two large β and β′ subunits that form the active site, two regulatory α subunits, and an ω subunit that supports RNAP assembly (Darst, 2001). This core enzyme cooperates with transcription factors and responds to signals on the DNA template and the nascent RNA to achieve full functionality *in vivo*. For example, elongating RNAP frequently enters an elemental paused state that can be stabilized by an RNA hairpin invading the RNA exit tunnel or by RNAP backtracking (Zhang and Landick, 2016). RNA synthesis is terminated intrinsically when the transcription elongation complex (TEC) transcribes a stable RNA hairpin followed by a uridine-rich stretch or with the aid of transcription termination factor ρ (Ray-Soni et al., 2016). Pausing and termination can be modulated by elongation factors, such as N-utilization substances (Nus) A and G (Zhang and Landick, 2016).

The interplay of pausing, termination, and continued transcription (anti-termination) is a pervasive, gene-regulatory principle in bacteria, for example during transcription attenuation (Gollnick and Babitzke, 2002) or transcriptional riboswitching (Sherwood and Henkin, 2016), where the outcome is decided during transcription of a short regulatory region. Alternatively, some regulators can stably insulate RNAP from the destabilizing effects of terminators over long distances. These processes are referred to as processive anti-termination (Weisberg and Gottesman, 1999) and can be elicited by RNA elements, such as the polymerase utilization (*put*) signal of phage HK022 (King et al., 1996) in *Escherichia coli*. Most lambdoid phages exploit an alternative mechanism of processive anti-termination during their lytic life cycles; this depends on a phage-encoded transcription factor, N, and an N-utilization (*nut*) site on the nascent phage RNA, composed of a linear sequence, *boxA*, and a hairpin element, *boxB*. N is produced as an immediate early gene product, binds *nut boxB*, and recruits four host transcription factors, NusA, NusB, NusE (equivalent to ribosomal protein S10), and NusG. These factors assemble a ribonucleoprotein complex (RNP) that accompanies RNAP during further transcription (Nudler and Gottesman, 2002). N/Nus-factor/*nut* RNA-modified RNAP resists pause and termination signals several kilobase pairs downstream of the modification site (Mason et al., 1992).

N-based processive anti-termination has been investigated since the 1960s and has served as a paradigm for transcription regulation. N of phage λ (λN) was one of the first factors discovered that exhibited anti-termination activity and that controlled RNAP during transcription elongation instead of initiation (Roberts, 1969). It also provided an example for RNAP control via a regulatory element on the RNA instead of on the DNA and illustrated spatial separation of the sites of effector recruitment and action as well as effector-based enlistment of host transcription factors. We recently worked out the global architecture of a λN-based transcription anti-termination complex (λN-TAC)

(Said et al., 2017), but the low resolution of this structure (10 Å) precluded visualization of the atomic-level details necessary to understand how λN counteracts diverse modes of pausing and termination. Here, we describe a 3.7 Å-resolution single-particle cryo-electron microscopy (cryo-EM) structure of a complete λN-TAC and structure-guided functional analyses, which portray a remarkable multi-pronged molecular strategy implemented by the small, intrinsically unstructured λN protein to re-program the *E. coli* transcriptional apparatus.

RESULTS

λN Reinforces the Elongation-Competent Conformation of RNAP

We subjected a recombinant λN-TAC comprising RNAP, a nucleic acid scaffold with an artificial transcription bubble and a consensus *nut* site on the RNA (Figure 1A), all Nus factors, and λN to single-particle cryo-EM analysis (Figures S1–S3), and we obtained a structure at a nominal resolution of 3.7 Å (Figure S2A; Table 1). Small variations compared to our previous assembly protocol (Said et al., 2017) and recording a larger dataset on a more modern electron microscope led to the improved resolution. The local resolution varied between 3.4 Å for the best-defined regions in the RNAP core to 12 Å surrounding the λN-Nus factor-*nut* RNP (the "modifying RNP"; Figure S2C). The latter components could be unequivocally placed into the cryo-EM map based on the crystal structure of a λN-NusA-NusB-NusE-*nut* RNA complex (Said et al., 2017) and the NMR structure of a NusG C-terminal domain (CTD)-NusE complex (Burmann et al., 2010). All elements directly contacting RNAP were clearly defined in the cryo-EM map and could be modeled *de novo* (Figure S2D).

In the λN-TAC, the modifying RNP is anchored next to the RNA exit tunnel of RNAP (Figure 1B; Video S1). RNAP exhibits a conformation very similar to that of an unmodified TEC (Kang et al., 2017) (root-mean-square deviation of 1.46 Å for 2910 common Cα atoms; Figure S4). Although the nucleic acid scaffold employed could form a pause-inducing 10-base-pair (bp) hybrid (Figure 1A), the λN-TAC encompasses an elongation-competent 9-bp hybrid that resides in the post-translocated state, with an unpaired +1 position in the DNA template strand, ready to receive an incoming nucleoside triphosphate (NTP; Figure 1C). We monitored run-off transcription by the assembled λN-TAC used for cryo-EM analysis in comparison to a complex lacking λN. λN-TAC yielded run-off products at a higher yield and at an increased rate compared to a TEC lacking λN (Figure 1D), showing that λN stabilizes the elongation-competent conformation of RNAP.

The Modifying RNP Is Flexibly Anchored to RNAP

The lower resolution of the cryo-EM map in the region corresponding to the upper modifying RNP suggests that this part of the complex is flexibly anchored to RNAP. Further classification of the particle images led to three sub-structures at nominal resolutions between 4.2 and 4.8 Å. In these structures, the main portion of the modifying RNP occupied two positions relative to RNAP, distributed around the position obtained from the complete map (Figure S3; Video S2). Comparison of these states suggests a bi-modal movement of the upper RNP as a rigid body. A "shake" of ~20° and a "nod" of ~10° about the base of the modifying RNP take the *nut boxB* edge either closer to or further away from the RNAP RNA exit tunnel.

In all conformational states, four components of the modifying RNP establish links to RNAP (Figure 1B; Video S1): (1) an about 37 Å-long α helix in the central part of λN (α3) runs along the upstream DNA duplex and the RNAP β flap tip (FT); (2) the NusA N-terminal domain (NTD) binds the other side of the FT; (3) the nascent RNA runs from the RNA exit tunnel of RNAP to *nut boxB* of the modifying RNP; and (4) the NusG NTD binds across the RNAP active site cleft, while its CTD abuts the NusA and NusE subunits of the modifying RNP. These bridging molecular elements are crucial for stabilizing the active conformation of RNAP and for countering diverse modes of pausing and termination as further detailed below.

λN Remodels the RNAP β Flap Tip

The NusA NTD is connected by an α helix to an array of one S1 and two hnRNP K homology (KH) RNA-binding domains, which are followed by two acidic repeat domains (AR1 and AR2) that are not universally conserved. In the λN-TAC, helix α1 of $NusA^{NTD}$ (residues 2–10), the NTD-S1 linker helix (residues 122–132), and the central helix α3 of λN (residues 58–82) form a tripod that engages the RNAP β FT (residues 887–915) like a push button (Figure 2A). The NusA/λN-FT interaction buries ~1,800 A^2 of combined surface area and is stabilized by hydrophobic interactions surrounded by hydrophilic contacts. These interactions stabilize a specific conformation of the FT, as the FT is disordered in an unmodified TEC (Kang et al., 2017).

In the absence of λN, interactions of the FT (Kang et al., 2018a; Toulokhonov and Landick, 2003) and the β′ Zinc-binding domain (ZBD; residues 35–107) (Epshtein et al., 2007; Gusarov and Nudler, 2001) with RNA hairpins increase pause lifetime and modulate intrinsic termination. Compared to recent cryo-EM structures of *his* operon hairpin-paused elongation complexes lacking (*his*PEC) or containing (NusA-*his*PEC) NusA (Guo et al., 2018; Kang et al., 2018a), the present structure reveals that λN helix α3 remodels the conformation of the FT and its contacts to the ZBD and NusA NTD (Figure 2B). The remodeled FT occupies a surface on the ZBD that accommodates the 3′ branch of the hairpin in *his*PECs, redirects RNA-binding residues R47 and K50 of the ZBD to the upstream DNA duplex and other parts of the ZBD, respectively, and hinders the tip of the hairpin from approaching the NusA NTD (Figure 2C). Moreover, E892 of the FT contacts ZBD K66 (Figure 2C, bottom), which interacts with the 3′ branch of pause hairpins in *his*PECs. Thus, λN-induced FT remodeling prevents RNA hairpin accommodation between the FT and ZBD, hinders the hairpin tips from approaching the NusA NTD-S1 region, and sequesters residues of the ZBD important for pausing and intrinsic termination.

λN-Mediated Remodeling Alters αCTD-NusA Interactions

Hairpin-stabilized pausing (Ha et al., 2010; Kolb et al., 2014) and intrinsic termination (Gusarov and Nudler, 2001) are further stimulated by NusA, presumably because the NTD and S1 domain can cradle the upper portions of RNA hairpins close to the rim

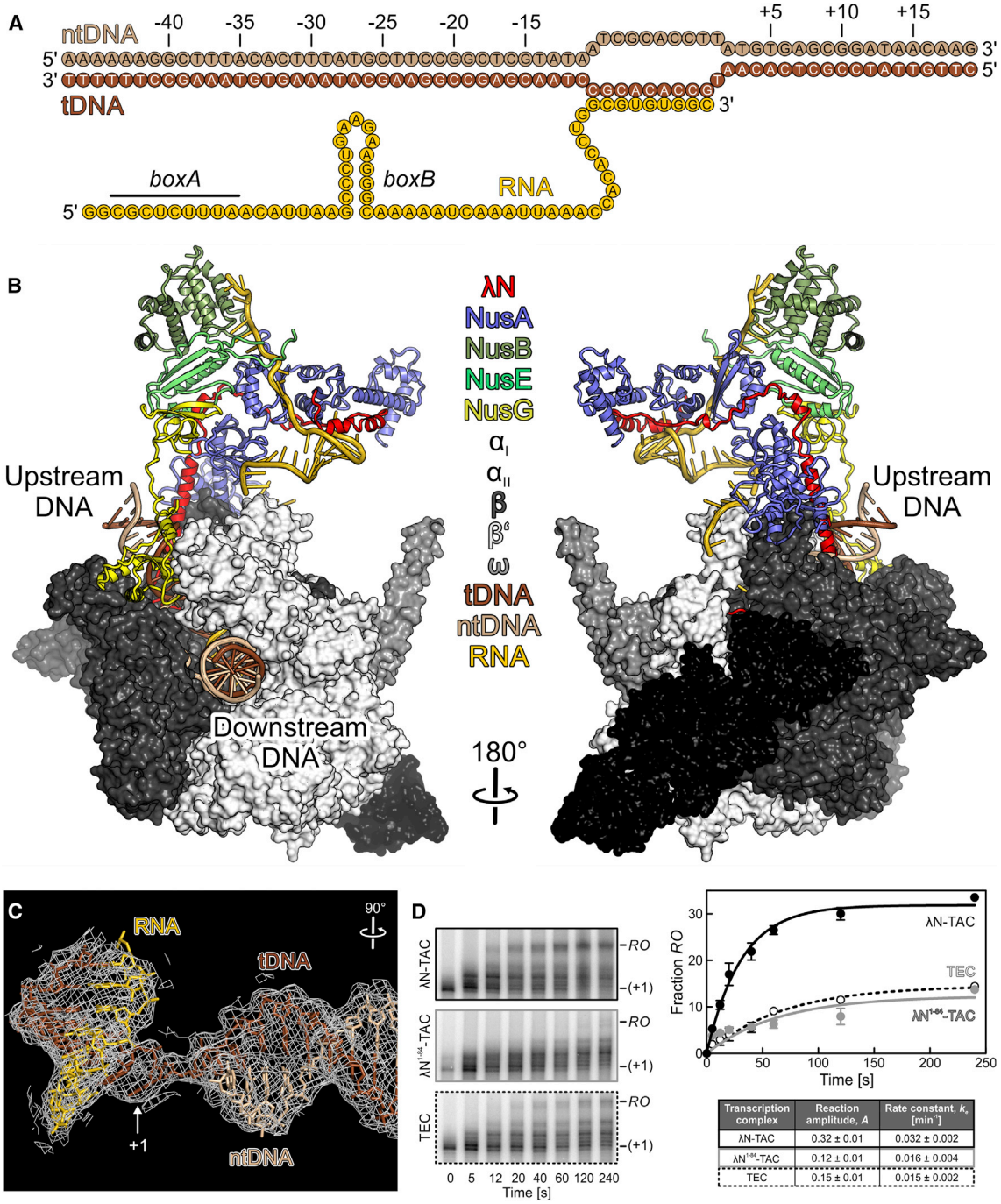

Transcription complex	Reaction amplitude, *A*	Rate constant, k_e [min^{-1}]
λN-TAC	0.32 ± 0.01	0.032 ± 0.002
λN$^{1-84}$-TAC	0.12 ± 0.01	0.016 ± 0.004
TEC	0.15 ± 0.01	0.015 ± 0.002

Figure 1. Structural Overview and Activity of the Assembled λN-TAC

(A) Nucleic acid scaffold employed in the structural analysis.

(B) λN-TAC with nucleic acids and the modifying RNP shown in cartoon mode and RNAP in surface representation. Color-coding of subunits is maintained in the following figures. tDNA, template DNA strand; ntDNA, non-template DNA strand.

(C) Cryo-EM map around the downstream DNA and the hybrid. The λN-TAC resides in the post-translocated state and the unpaired +1 position of the template strand is indicated. Rotation symbols in this and the following figures indicate the view relative to Figure 1B, left.

(D) Run-off transcription by the *in vitro* assembled λN-TAC used for cryo-EM analysis, a TEC lacking λN, and a λN-TAC bearing a truncated version of λN (residues 1–84). +1, addition of the first nucleotide; *RO*, run-off product. Data were fit to a first-order reaction (fraction $RO = A[1-\exp(-k_e\,t)]$; *A*, amplitude of the reaction; k_e, apparent first-order rate constant of elongation; t, time). Quantified data (right) represent means ± SD of three independent experiments. See also Figures S1–S4 and Videos S1 and S2.

Table 1. Cryo-EM Data Collection and Refinement

Data Collection	
Pixel Size (Å/px)	0.675
Defocus range (μm)	0.75–3.3
Voltage (kV)	300
Electron dose e^{-}/A^{2}	69
Number of frames	40
Micrographs total/used	4,074/3,550
Particle images total/used	802,858/708,030
Refinement	
Resolution $FCS_{0.143}$ (Å)	3.7
Map sharpening B-factor (A^{2})	−97
CC mask	0.791
CC volume	0.787
Model composition Non-hydrogen atoms Protein residues DNA residues RNA residues Zn^{2+}/Mg^{2+} ions	34797 4274 52 47 2/1
Rmsd from ideal geometry Bond lengths (Å) Bond angles (°)	0.007 0.919
Ramachandran plot Favored (%) Allowed (%) Outliers (%)	92.2 7.73 0.07
Model quality[a]: Clash score	5.73
Model quality[a]: Rotamer outliers	0.25
Model quality[a]: Overall score	1.79

[a]Assessed using MolProbity (Chen et al., 2015)

of the RNA exit tunnel (Guo et al., 2018). λN helix α3 and the following region further connect to the base of the β flap (residues 830–1058) and β protrusion (residues 450–507; Figure 2A), leading to global repositioning of NusA compared to a NusA-*his*PEC (Guo et al., 2018) (~45° rotation about the beginning of the NusA NTD-S1 linker helix; Figure 2D). N-terminal portions of λN, *nut* site RNA, the NusB-NusE dimer, and the NusG CTD encircle distal parts of NusA and pull them into the direction of the upstream DNA duplex (Figure 2D).

As λN appears to serve as the key connector between the elements surrounding NusA, we tested the relevance of this global remodeling by surveying the consequences of systematic λN truncations in an *in vitro* anti-termination assay. Deleting the first 37 residues of λN ($\lambda N^{38–107}$), which together with *nut boxB* bind the NusA KH domains, reduced anti-termination by about 25% (Figure 2E, lanes 4 and 5), and anti-termination was entirely lost upon deletion of the first 57 residues ($\lambda N^{58–107}$), including λN-NusE contacts (Figure 2E, lanes 4 and 6). About 60% of the anti-termination activity remained upon deletion of the C-terminal 22 residues of λN ($\lambda N^{1–84}$; Figure 2E, lanes 4 and 8), but anti-termination was again essentially lost when helix α3 was additionally deleted ($\lambda N^{1–62}$; Figure 2E, lanes 4 and 9). These results support the essential role of λN helix α3 in NusA repositioning and underscore the importance of neighboring λN regions that anchor it to other components in the modifying RNP (N-terminal of helix α3) and to RNAP (C-terminal of helix α3).

In a NusA-*his*PEC, NusA NTD and AR2 contact the CTDs of the RNAP α subunits, and the NusA KH domains rest on the tip of the ω subunit (Guo et al., 2018; Figure 2D). αCTDs and NusA AR2 lack density in the λN-TAC cryo-EM map, suggesting that αCTD-NusA interactions are broken during λN-mediated repositioning of NusA (Figure 2D). Consistent with this notion and previous data (Liu et al., 1996; Mah et al., 1999), removal of both αCTDs or NusA AR2 did not affect λN-based anti-termination (Figure 2F, lanes 3–5). While removal of NusA AR2 also did not strongly affect intrinsic termination by Nus factor-modified RNAP in the absence of λN (Figure 2F, lanes 6, 8, 9, and 11), NusA-enhanced intrinsic termination was strongly reduced upon removal of αCTDs in the absence of λN (Figure 2F, lanes 7 and 10), at least in part due to inefficient binding of NusA to TECs lacking αCTDs (Figure 2G). Therefore, λN replaces NusA-αCTD contacts that normally support NusA recruitment and intrinsic termination.

Guidance of Nascent RNA Might Oppose Hairpin Formation

The cryo-EM map for the RNA region connecting the RNA at the hybrid to *nut boxB* is fragmented. Density that appears at lower contour levels suggests that the exiting RNA runs across a positively charged surface of the FT and ZBD and along the NusA S1 domain (Figure 3A,B). Guided along this path, the upper branch of a nascent RNA hairpin would be prevented from pairing with the lower branch in the RNA exit tunnel, such that hairpin formation would be avoided or delayed until the entire hairpin has exited RNAP. Several positively charged residues surrounding the concave surface of the NusA S1 domain could provide suitable guidance for the RNA (Figure 3A). Indeed, deletion of the NusA S1 domain and all following regions ($NusA^{1–137}$) reduced anti-termination by about 50% (Figure 3C, lanes 4 and 5). Double alanine mutations of K143 and K144, which point away from the proposed RNA path (Figure 3A), had no effect on anti-termination (Figure 3C, lanes 4 and 6), while alanine mutations of R147 or R164, lining the proposed RNA path (Figured 3A and 3B), reduced anti-termination by 35% and 25%, respectively (Figure 3C, lanes 4, 7, and 8). Although the double RR147/164AA mutation did not further increase the effect (Figure 3C, lanes 4 and 9), these findings are consistent with the idea that λN-induced reorganization of RNAP RNA-binding elements and NusA provides for guidance of the exiting RNA that counteracts or delays hairpin folding.

Our mutational analyses might also support an additional function of NusA S1 residue R147. In the λN-TAC, NusA R147 reaches down to a loop (residues 85–88) of the ZBD (Figure 3A,B). Deletion of ZBD residues 70–88 significantly reduces intrinsic termination (King et al., 2004). Thus, λN-induced positioning of NusA S1 on top of the ZBD might lead to NusA R147 shielding ZBD regions important for intrinsic termination.

λN Lines Upstream DNA and the Hybrid and Stabilizes the Active State of RNAP

Opposite the FT, several positively charged residues (K65, R73, R76, R80, and K85) of λN helix α3 and the following loop face the

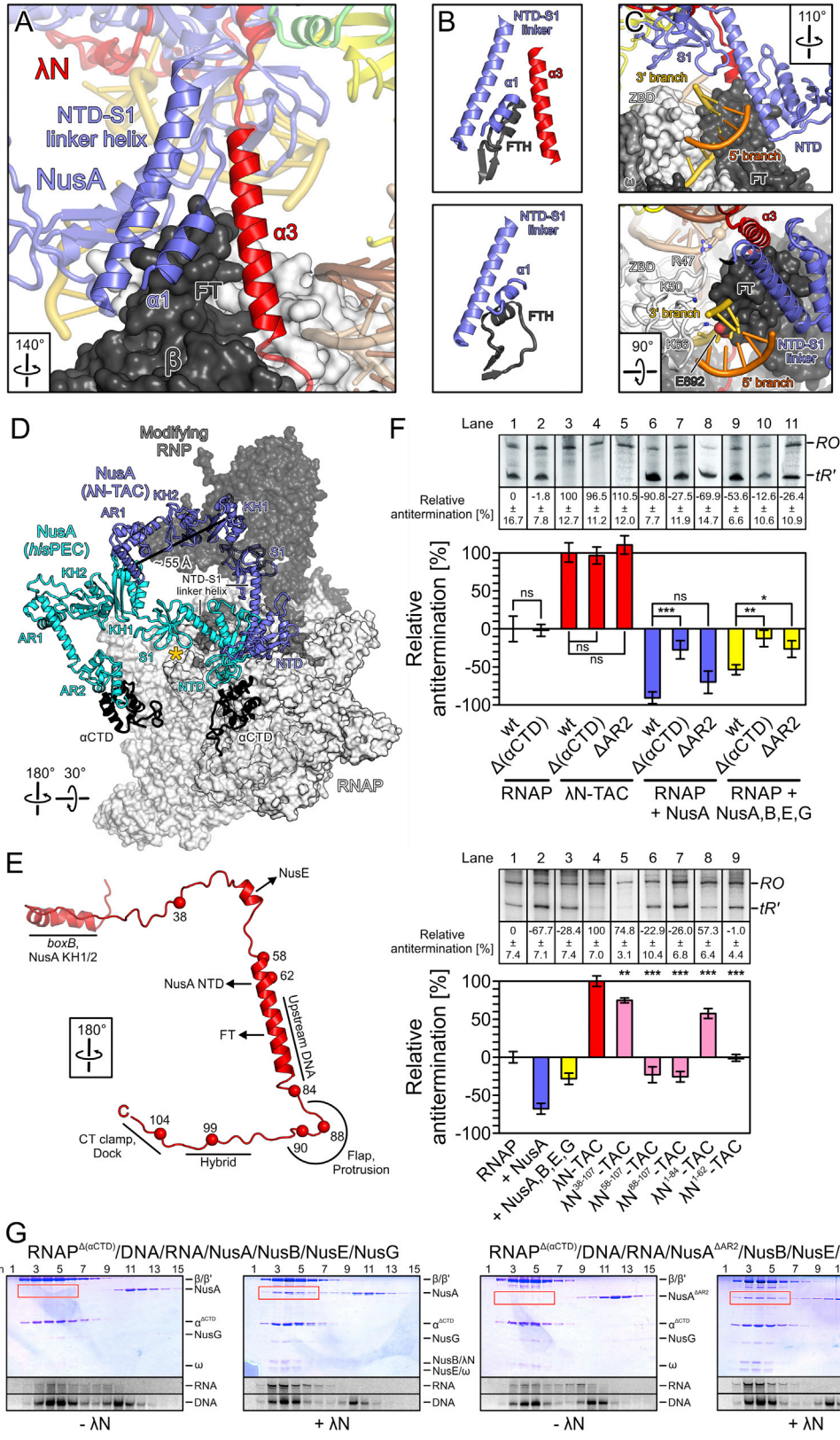

(legend on next page)

upstream DNA duplex (Figure 4A). The positively charged side chains shield negative charges of the DNA backbone, likely strengthening the duplex by reducing electrostatic repulsion between the DNA strands. The lower part of λN helix α3 (R76) and the following loop (K85) approach the template and non-template strands a full turn and half a turn, respectively, upstream of their site of re-engagement (Figure 4A). Thus, λN helix α3 might reinforce base pairing upstream of the transcription bubble, which would counteract RNAP backtracking.

Strikingly, following helix α3, λN meanders along the β flap (residues 1039–1048) and the β protrusion, enters the RNAP hybrid cavity, and traverses the hybrid to the RNA exit tunnel (Figure 4B). λN snakes through existing crevices in the TEC (Kang et al., 2017) and does not induce major distortions in RNAP or the hybrid, except for a slight upward movement of the β flap and β′ clamp elements covering the hybrid. Entry into paused states is accompanied by swiveling of a β′ module (clamp, dock, shelf, SI3, and CTR) (Kang et al., 2018a). Interestingly, on its way through the catalytic cavity, λN links some of these mobile elements to other parts of RNAP, likely counteracting pause-associated conformational changes.

The end of λN helix α3 is fixed to the base of the β flap by λN W82/Y83 stacking on a loop of the β flap (residues 1039–1048), and by λN Y83 and S84 hydrogen bonding with the main and side chains of β D842 and R936, respectively (Figure 4C). The following λN residues 84–94 further encircle the loop of the β flap, on which λN W82/Y83 stacks, with λN residues 88–92 contacting the β protrusion (Figure 4C). Beyond residue 92, λN runs between the backside of the β flap and the hybrid (Figure 4D). Positively charged side chains extend toward the hybrid (K98, K100) and the exiting RNA (K102; Figure 4D). This configuration suggests that λN counteracts hybrid melting, and thus termination, by decreasing the inner diameter of the hybrid cavity and by reducing charge repulsion between the paired DNA and RNA. λN residues 99–105 lie underneath the β′ lid (residues 250–264) and interconnect the β flap and the C-terminal clamp region of β (CT clamp; residues 1,233–1,342; Figure 4B).

The C-terminal ten residues of λN rest between the CT clamp and the β′ dock (residues 369–420), lining the exit tunnel opposite the ZBD (Figure 4E). Superposition of *his*PECs (Guo et al., 2018; Kang et al., 2018a) and the λN-TAC based on the RNAP cores revealed that the 3′ branch of a hairpin could, in principle, still be accommodated next to the λN-remodeled FT, albeit displaced from the ZBD and NusA NTD (Figure 4E). However, the 5′ branch of a hairpin would then clash with the C terminus of λN (Figure 4E). Apart from constricting the diameter of the RNA exit tunnel, cross-strutting of the β CT clamp and β′ dock by the λN C terminus likely counteracts widening of the exit tunnel associated with RNAP swiveling (Kang et al., 2018a).

To directly test the importance of the above λN contacts, we monitored the effects of specific λN residue substitutions on intrinsic termination. Alanine mutations of R76/R80/K85 (lining the upstream DNA), W82/Y83 (fixing helix α3 at the base of the β flap), R89 or R89/R96 (contacting the β protrusion), R96/K98 (contacting the β protrusion [R96] and pointing to the hybrid [K98]), or K98/K100/K102 (pointing to the hybrid [K98, K100] and to the exiting RNA [K102]) led to a loss of 15%–50% of anti-termination activity (Figure 4F, lanes 4–10), with combinations of mutations showing stronger effects than single mutations. Moreover, anti-termination activity of λN-modified RNAP (in the absence of Nus factors) was decreased stepwise by incremental C-terminal deletions of λN, which sequentially removed contacts to the CT clamp and dock ($\lambda N^{1–104}$ and $\lambda N^{1–99}$; Figure 4F, lanes 13–14), β flap ($\lambda N^{1–90}$; Figure 4F, lane 15) and the β protrusion ($\lambda N^{1–84}$; Figure 4F, lane 16). Finally, a C-terminal peptide of λN ($\lambda N^{88–107}$), containing the elements that run through the hybrid cavity, significantly increased anti-termination activity of otherwise unmodified RNAP (Figure 4F, lane 17).

Figure 2. Remodeling of the FT and Repositioning of NusA

(A) Interaction of two N-terminal helices of NusA (blue) and of the central α3 helix of λN (red) with the RNAP FT (gray surface).

(B) Comparison of the NusA-λN-FT interaction in the λN-TAC (top) and the NusA-FT interaction in a NusA-*his*PEC (PDB ID 6FLQ) after superposition according to the NusA NTD-S1 linker helix.

(C) Two views on a pause hairpin in the RNA exit tunnel modeled on the λN-TAC by superposition of a NusA-*his*PEC (PDB ID 6FLQ) according to the NusA subunits. The remodeled FT interferes with positioning of the 3′ branch (gold) of the hairpin on the ZBD and with its tip approaching the NusA NTD (top). It also redirects RNA-binding residues of the ZBD to upstream DNA or other regions of the ZBD (bottom). Color coding for residues shown as sticks in this and the following figures: carbon, as the respective protein subunit; nitrogen, blue; oxygen, red. Black dashed lines in this and the following figures, hydrogen bonds, salt bridges, or contacts.

(D) Global repositioning of NusA (blue) by λN and other portions of the modifying RNP (gray semitransparent surface), illustrated by the position of NusA in a NusA-*his*PEC (PDB ID 6FLQ; cyan) modeled on the λN-TAC by global superposition of the RNAPs. RNAP αCTDs (black) as seen in the NusA-*his*PEC are also shown. RNAP and nucleic acids, light gray surface. Black line, distance between equivalent points in the NusA KH1 domains. Golden asterisk, position of the tip of the pause hairpin in the NusA-*his*PEC.

(E) Left: ribbon plot of λN highlighting truncation positions and interacting elements in the λN-TAC. Right: transcription assays monitoring anti-termination efficiency 3-min time points. Transcription complexes are indicated at the bottom, and products are identified on the right: *RO*, run-off transcript; *tR′*, transcript terminated at *λtR′*. Samples were analyzed on several identical gels, and duplicate lanes were removed for display. Relative anti-termination in this and the following figures was calculated by setting anti-termination efficiency of RNAP alone to 0% and of λN-TAC to 100% and scaling quantified data for other complexes accordingly. Quantified data represent means ± SD of three independent experiments. Significance is relative to λN-TAC. Significance indicators in this and the following figures: *, $p < 0.05$; **, $p < 0.01$; ***, $p < 0.001$; ns, not significant ($p \geq 0.05$).

(F) Effect of deletion of αCTDs or NusA AR2 on RNAP (lanes 1 and 2), λN-TAC (lanes 3–5), NusA-modified RNAP (lanes 6–8), and a TEC lacking λN (lanes 9–11) analyzed in the same fashion as in (E). Transcription complexes and factor variations are identified at the bottom.

(G) Coomassie-stained SDS-PAGE (proteins; top) and ethidium bromide-stained urea PAGE (nucleic acids; bottom) analyses of size-exclusion chromatography runs showing lack of efficient incorporation of NusA or $NusA^{\Delta AR2}$ into a TEC lacking λN and αCTDs (first and third sections), but efficient binding of NusA or $NusA^{\Delta AR2}$ in the presence of λN (second and fourth sections). Presence of λN is indicated below the gels; mixtures of other components loaded in each run are indicated above the gels. Bands are identified on the right. Expected positions of NusA/$NusA^{\Delta AR2}$ in the complexes are indicated by red boxes. In the absence of λN, there is also inefficient incorporation of the NusB-NusE dimer.

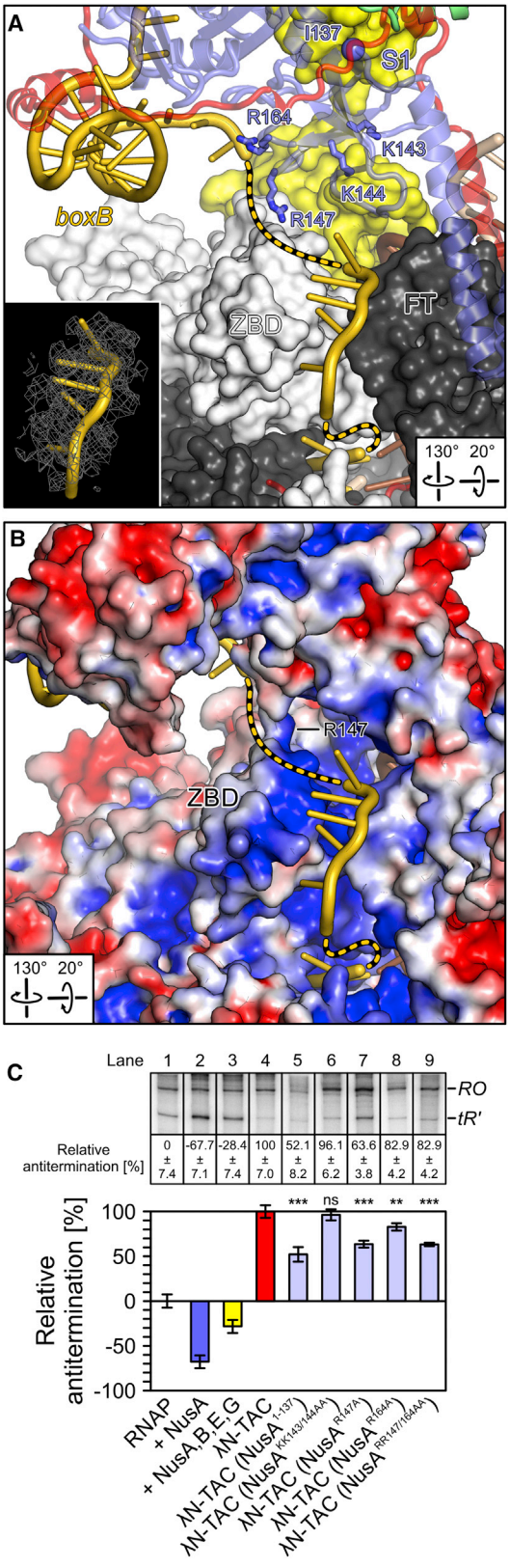

Figure 3. Chaperoning RNA in an Extended Conformation

(A) Path of the transcript from the RNA exit tunnel to the *boxB* element across the ZBD and FT and along the NusA S1 domain (NusA AR2 omitted). Golden dashed lines, regions of the RNA not defined in the cryo-EM map; sphere, site of NusA truncation for the experiment shown in (C), lane 5. Side chains of positively charged residues around the concave surface of the NusA S1 domain, which were mutated for functional tests in (C), are shown as sticks. Inset, cryo-EM map at the 4σ level around the RNA portion between ZBD and FT.

(B) Electrostatic surface potential of the protein components of the λN-TAC, illustrating possible guidance of the exiting RNA along positively charged surface regions. Compared to (A), NusA AR2 is included and partially occludes RNA regions in the back.

(C) Transcription assays monitoring anti-termination efficiency at 3-min time points by the transcription complexes indicated at the bottom. Products are identified on the right: *RO*, run-off transcript; *tR'*, transcript terminated at λ*tR'*. Samples were analyzed on several identical gels, and duplicate lanes were removed for display. Quantified data represent means ± SD of three independent experiments. Significance relative to λN-TAC. Lanes 1–4 are identical to Figure 2E, lanes 1–4.

Thus, the observed interactions of λN with different parts of RNAP and nucleic acids in the hybrid cavity seem to contribute additively to λN-based anti-termination activity.

λN Might Communicate with the RNAP Active Site

Previous analyses had suggested that pause hairpins affect the RNAP active site via the β connector (residues 814–839 and 1048–1065; Toulokhonov et al., 2001), a two-stranded β sheet that links the β flap to the active site. Residues 93–98 of λN run across the upper portion of the connector, and C-terminal λN residues intervene between the connector and RNA in the exit tunnel (Figure 4D). Thus, λN might directly influence RNAP activity via the connector and undermine signaling from exit tunnel RNA to the active site. Consistent with this notion, the yield and rate of run-off transcription of a λN-TAC bearing λN^{1-84} were strongly reduced compared to an intact λN-TAC and were similar to those of a TEC lacking λN entirely (Figure 1D).

λN Enhances Anti-pausing and Anti-termination Activities of NusG

The NusG NTD locks the nucleic acids in the active center cleft by bridging between the lateral walls (Figure 5A), as also seen in a recent cryo-EM structure of a NusG-modified TEC (Kang et al., 2018b). NusG helix α1 (residues 18–33) runs along the β protrusion, helix α2 (residues 77–84) rests on the β gate loop (residues 359–388), the loop preceding helix α3 (residues 94–101) is wedged between the β gate loop and N-terminal parts of the β′ clamp (residues 132–190), and an exposed edge of the NTD's central β sheet together with helix α3 (residues 105–117) provides a platform for the tip of the β′ clamp helices (residues 265–307; Figure 5B). As pointed out before (Kang et al., 2018b), these contacts could explain anti-pausing activity of NusG by counteracting RNAP swiveling.

In the λN-TAC, NusG residues F15, S16, F18, and R21 (loop preceding helix α1) contact the template and non-template strands, guiding them close together directly after separation of the template strand from the nascent RNA; in addition, a long loop (residues 53–62) of the NusG NTD that is flexible in isolation (Mooney et al., 2009) lines the major groove of the

Please cite this article in press as: Krupp et al., Structural Basis for the Action of an All-Purpose Transcription Anti-termination Factor, Molecular Cell (2019), https://doi.org/10.1016/j.molcel.2019.01.016

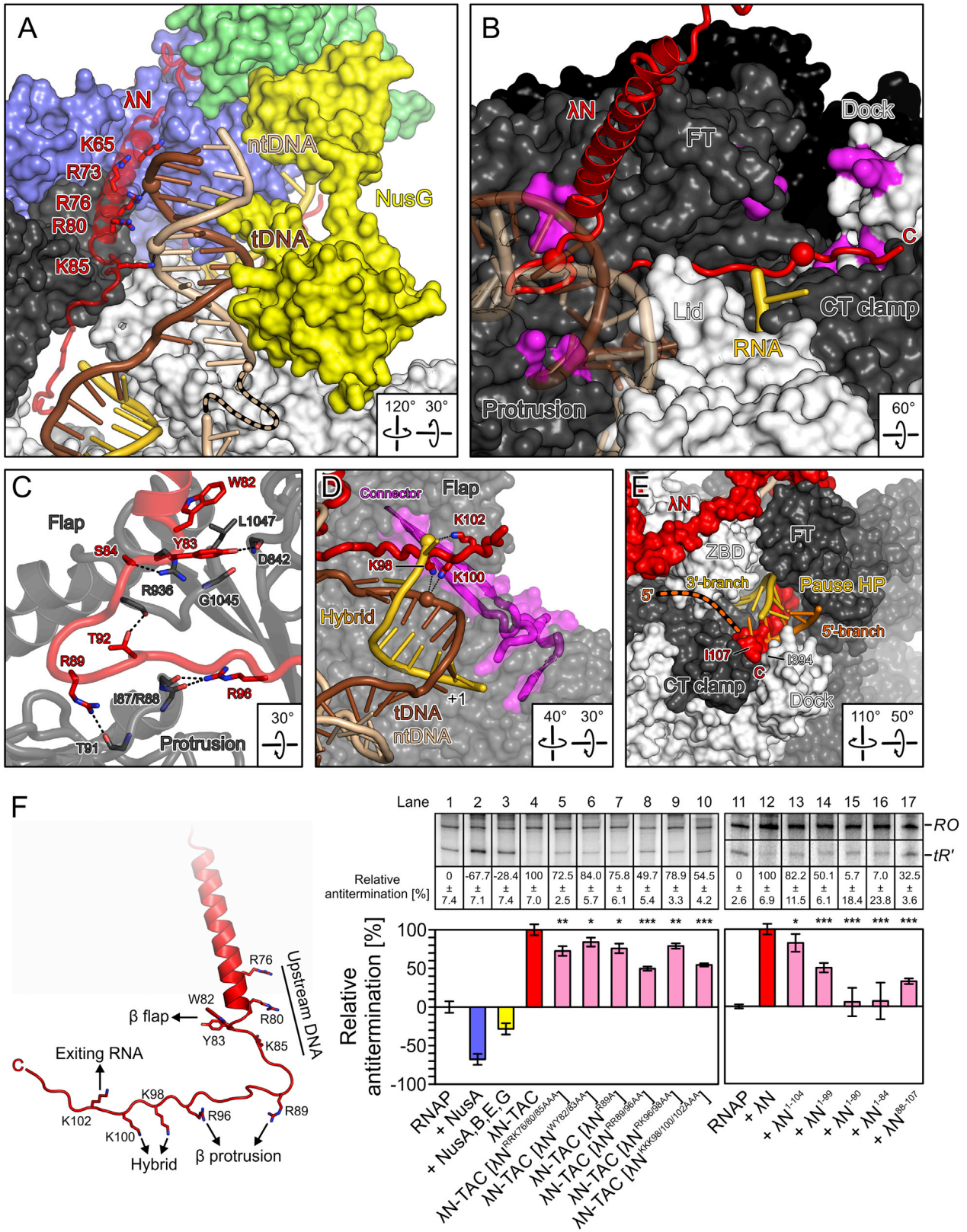

(legend on next page)

upstream DNA duplex in the λN-TAC (Figure 5C). These structural features rationalize how NusG counteracts RNAP backtracking (Herbert et al., 2010) and support re-annealing of the first nucleotide after the transcription bubble (Turtola and Belogurov, 2016).

Backtracking and swiveling may be countered more efficiently by the NusG paralog RfaH than by NusG due to the more extensive contacts of the NusG-like RfaH NTD to upstream DNA (Kang et al., 2018b) (Figure 5D). In the λN-TAC, λN runs along the upstream DNA duplex opposite of NusG, holding the DNA close to NusG (Figure 5C) and thus likely enhancing its anti-backtracking, re-annealing, and anti-swiveling activities. Moreover, in contrast to the NusG CTD in the λN-TAC, the RfaH CTD binds the RNAP β flap tip, which might counteract hairpin-stabilized pausing (Figure 5D); in the λN-TAC, this role is played by the central α3 helix of λN, although the FT is positioned differently in the λN-TAC than in RfaH-modified RNAP. Thus, λN seems to make up for multiple anti-pausing and anti-termination deficits of NusG compared to RfaH.

A NusA-NusG^{CTD}-NusE Interaction Inhibits ρ-Dependent Termination

The NusB-NusE dimer binds *nut boxA* in the modifying RNP (Figure 1B). A flexible linker connects the NusG NTD to the CTD, allowing the CTD to be positioned between the NusA S1 domain and NusE via an interaction network involving NusG F144 and F165; NusA T139, V141, R178, and R180; and NusE M88, D91, and L92 (Figures 6A and 6B). While the NusG^{CTD}-NusE interaction resembles a previous NMR structure of an isolated NusG^{CTD}-NusE complex (Burmann et al., 2010), the interaction with NusA has not been described previously.

The NusG CTD also binds transcription termination factor ρ, an RNA-dependent NTPase that can engage transcripts at pyrimidine-rich ρ-utilization (*rut*) sites, translocate on the RNA, and disassemble the TEC upon encounter of RNAP. The NusG CTD enhances ρ engagement of *rut* sites, but interactions of the NusG CTD with NusE and ρ are mutually exclusive (Lawson et al., 2018). Our results suggest that additional interactions of NusG^{CTD} with NusA^{S1} likely contribute to ρ exclusion. To test whether the NusA^{S1}-NusG^{CTD}-NusE interaction counteracts ρ-dependent termination, we conducted *in vitro* ρ-dependent termination assays. λN-TAC transcribed through a ρ-dependent terminator irrespective of the presence of the NusG CTD (Figure 6C, lanes 7–10). In contrast, no anti-ρ activity was seen in the absence of λN (Figure 6C, lanes 1–4), but under these conditions, ρ activity was partially suppressed upon deletion of the NusG CTD (Figure 6C, lanes 5–6). When not repositioned by λN, NusA^{S1}, and NusE are too far away from the NusG NTD for the NusG CTD to reach (Figure 6D). Moreover, NusE will likely not join TECs in the absence of a *boxA* element, and the relative orientation of Nus factors on *nut* RNA is most likely not maintained in the absence of λN, such that NusA^{S1} and NusE would fail to form a binding pocket for NusG^{CTD}. While positioning of NusA^{S1} and NusE by λN generates an efficient sequestration site for NusG^{CTD}, λN elicits additional anti-ρ effects, as it suppresses ρ activity more efficiently than deletion of the NusG CTD (Figure 6C, lanes 6 and 8). Although the binding site of ρ on RNAP is presently unknown, we note that RNA contacts of λN-repositioned NusA^{S1} or the bulk of the modifying RNP could hinder ρ from approaching its functional binding site on RNAP.

DISCUSSION

The λN-TAC Structure Rationalizes Numerous Previous Observations

We resolved the structure of the λN-modified anti-termination complex at high resolution and revealed interactions of λN with the transcriptional machinery that likely explain how λN renders RNAP pause- and termination-resistant. Our results fully rationalize results from more than five decades of research on this mechanism. For instance, our findings provide explanations for the N-induced alteration of nascent RNA interactions by the FT, the ZBD, and NusA (Cheeran et al., 2007; Gusarov and Nudler, 2001); the importance of the flexible arms of the FT (residues 890–899 and 910–914) (Toulokhonov et al., 2001; Toulokhonov and Landick, 2003) and of ZBD residues 50–52 (Epshtein et al., 2007) for intrinsic termination; UV-induced crosslinks of a terminator hairpin to the NusA S1 domain in a λN- and NusA-modified TEC (Gusarov and Nudler, 2001); N-mediated destabilization of pause or terminator hairpins (Cheeran et al., 2005); or N-dependent prevention of RNAP backtracking (Cheeran et al., 2007). The unexpected path of λN through the hybrid cavity explains results from

Figure 4. Interactions Involving the Central and C-Terminal Portions of λN

(A) λN helix α3 running along upstream DNA with positively charged side chains extending toward the DNA as sticks. Beige dashed line, gap in the cryo-EM map for the ntDNA.

(B) λN helix α3 interacting with the base of the flap and the protrusion, and C-terminal parts of λN traversing the hybrid cavity to the dock and CT clamp (ZBD and Nus factors omitted). Spheres, positions of λN K85 and K102 that can be chemically cross-linked to neighboring β and β′ residues (magenta) (Said et al., 2017).

(C) λN interacting with the flap and protrusion. Interacting residues are shown as sticks.

(D) λN running between the connector, exiting RNA and the hybrid (β′ omitted). Positively charged side chains extending toward the hybrid and exiting RNA are shown as sticks.

(E) The λN C terminus lining the RNA exit tunnel between the CT clamp and dock. The 5′ branch (orange) of a pause hairpin, modeled by superposition of a NusA-*his*PEC (PDB ID 6FLQ) according to the RNAPs, clashes with the C terminus of λN. Orange dashed line, presumed path of regions 5′ of the hairpin.

(F) Transcription assays monitoring anti-termination efficiency at 3-min time points by the transcription complexes indicated at the bottom. Products are identified on the right: *RO*, run-off transcript; *tR'*, transcript terminated at λ*tR'*. In lanes 11–17, RNAP alone was compared to RNAP in the presence of the indicated λN variants but in the absence of Nus factors, using a shorter template with a 73 nt distance between *tR'* and *RO*. Samples were analyzed on several identical gels, and duplicate lanes were removed for display. Due to the wider separation on the gels, space between bands representing *tR'* and *RO* in lanes 11–17 was removed as well. Quantified data represent means ± SD of three independent experiments. Significance is relative to λN-TAC (λN point mutations), RNAP-λN (λN C-terminal truncations), or RNAP alone (λN$^{88–107}$). Lanes 1–4 are identical to Figure 2E, lanes 1–4.

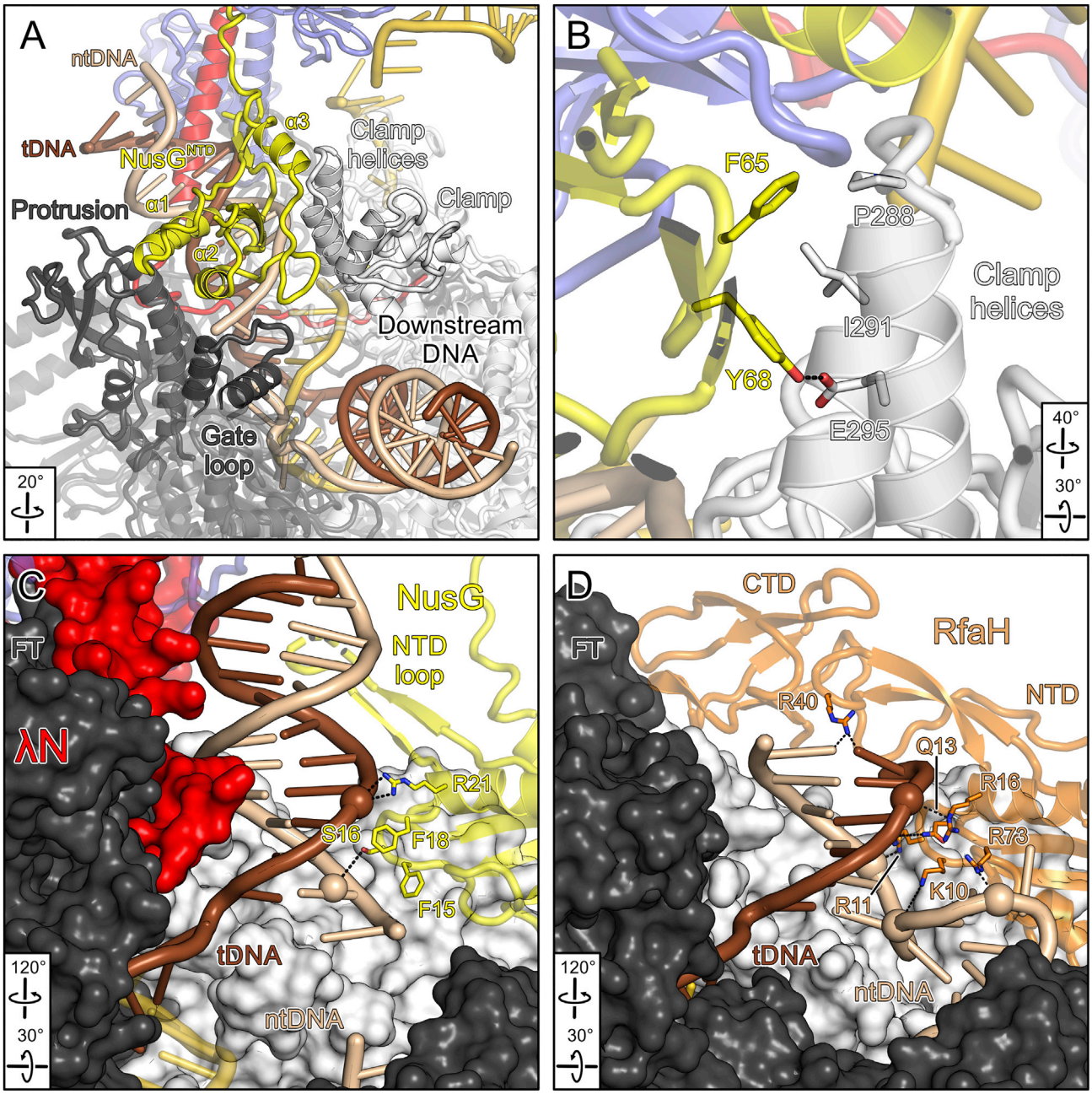

Figure 5. Cooperation of λN with NusG

(A) Interactions of the NusG NTD with the protrusion, gate loop, and clamp elements.

(B) NusG F65 and Y68 interacting with residues of the β′ clamp helices. Interacting residues are shown as sticks.

(C) NusG residues F15, S16, F18, and R21 interacting with upstream DNA, supporting formation of the first base pair after the template strand separated from the transcript. Interacting residues are shown as sticks. A long NTD loop lines the major groove of the upstream duplex.

(D) Comparison to an RfaH-bound TEC (PDB ID 6C6T).

previous cross-linking mass spectrometry (Said et al., 2017) and hydroxyl-radical footprinting (Cheeran et al., 2007) analyses. Observed λN contacts to the β flap (residues 1,039–1,048) and its path along the hybrid rationalize interference of a β G1045D mutation with N activity (Cheeran et al., 2005) and N-mediated stabilization of the hybrid (Cheeran et al., 2007; Parks et al., 2014), respectively. The increased RNAP elongation rate in the presence of λN is in line with the observed increased catalytic competence of RNAP and subtle changes around the active site in the presence of N proteins (Cheeran et al., 2007), and it may be mediated by N-connector interactions.

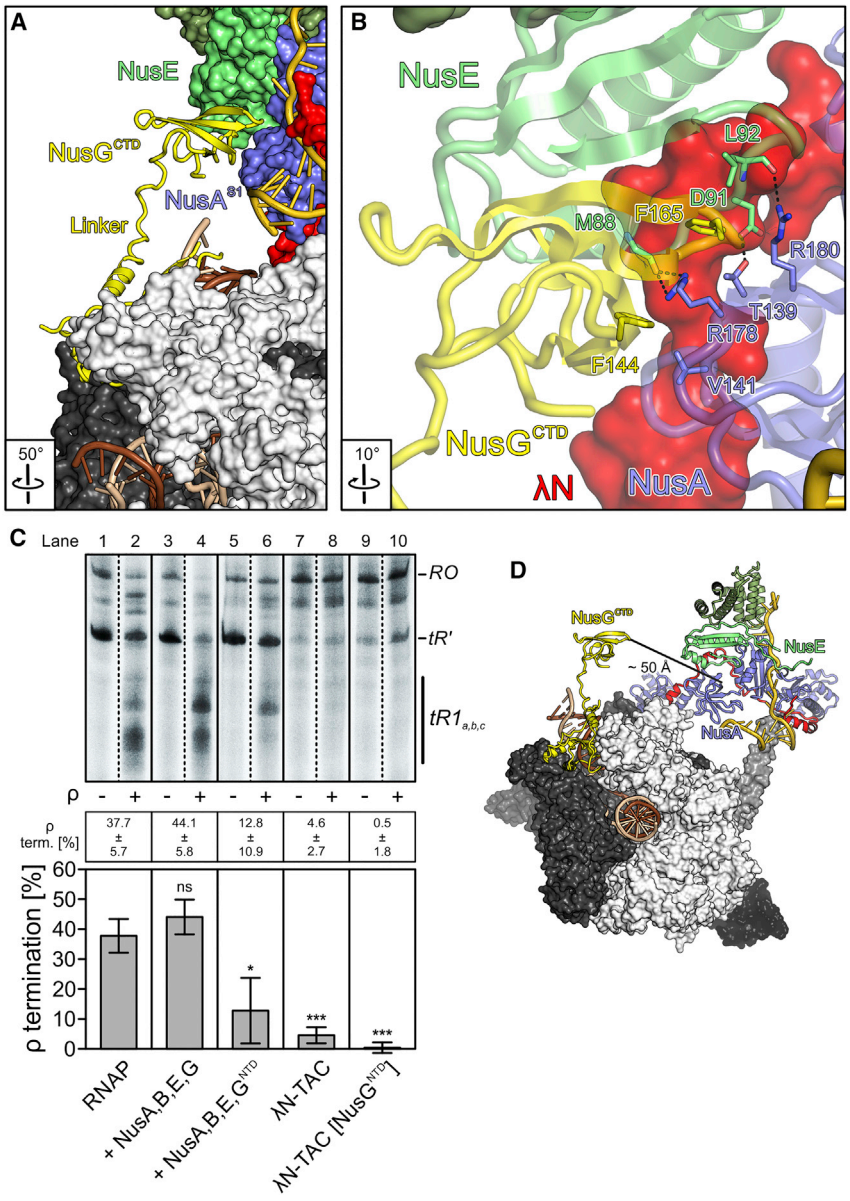

Figure 6. NusG CTD Interactions and Impact on ρ

(A) Binding of the NusG CTD at a NusA^{S1}/NusE pocket.

(B) Details of the NusA^{S1}-NusG^{CTD}-NusE interaction. Interacting residues are shown as sticks.

(C) Transcription assays monitoring termination in the λ*tR1*$_{a,b,c}$ region at 3-min time points by the transcription complexes indicated at the bottom in the absence or presence of ρ. The template encoded a *rut* site followed by ρ-dependent λ*tR1* and intrinsic λ*tR'* terminators. Products are identified on the right: *RO*, run-off transcript; *tR'*, transcript terminated at λ*tR'*; *tR1*$_{a,b,c}$, transcripts terminated in the λ*tR1*$_{a,b,c}$ region. Samples were analyzed on the same gel, but lanes were rearranged for display. ρ termination was calculated as the fraction of *tR1*$_{a,b,c}$ transcripts relative to all transcripts in a lane, corrected for the respective run lacking ρ. Quantified data represent means ± SD of three independent experiments. Significance is relative to RNAP alone.

(D) The λN-NusA-NusB-NusE-*nut* RNA complex modeled according to the positioning of NusA in a NusA-*his*PEC (PDB ID 6FLQ) by superposition of the NusA subunits.

to the ZBD and NusA NTD, as seen in *his*PECs and may sequester RNA-binding residues of the ZBD involved in hairpin accommodation. The very C terminus of λN remodels the opposite wall of the RNA exit tunnel, constricting the tunnel's inner diameter, which is expected to compete with alternative accommodation of regulatory hairpins and to counteract swiveling-associated exit tunnel opening.

Third, λN seems to stabilize RNAP and nucleic acids to promote processive elongation. Together with the NusG NTD, it binds upstream DNA, likely favoring DNA re-annealing and preventing RNAP backtracking and swiveling. C-terminal parts of λN that traverse the hybrid cavity may avert pause-related conformational changes of RNAP, stabilize the hybrid, functionally insulate the exit tunnel from the active site, and possibly enhance the catalytic activity of RNAP via contacts to the connector.

Thus, λN resembles a molecular "Swiss army knife" with numerous tools that counteract essentially all modes of pausing and termination. It will be interesting to see if, e.g., the Q protein of phage λ that installs a NusA-dependent shield against ρ-dependent and intrinsic termination (Shankar et al., 2007) and factors that form a TAC during ribosomal RNA synthesis (Belogurov and Artsimovitch, 2015) employ similar mechanisms.

Remarkably, λN can comprehensively reprogram RNAP and elongation factors, although it is a very small protein (107 residues). Our results show that, due to its intrinsic disorder (Van Gilst and von Hippel, 1997), it can adopt a highly elongated conformation that results in a large exposed interaction surface.

Intrinsic Disorder Allows λN to Implement a Multi-pronged Anti-pausing and Anti-termination Strategy

Our results suggest that λN can bestow pause and termination resistance on the transcriptional apparatus by three main mechanisms (Figure 7A). First, λN globally repositions NusA. Thereby, NusA regions that otherwise stabilize RNA hairpins in the exit tunnel are displaced; NusA-αCTD interactions that support hairpin-stimulated pausing and intrinsic termination are broken; exiting RNA is guided in a manner that might counteract or delay hairpin formation; access of ρ to its RNAP binding site might be obstructed; NusA S1 seems to shield surfaces on the ZBD important for intrinsic termination; and NusA^{S1} and NusE are brought into a position to sequester the NusG CTD from ρ.

Second, λN locally remodels RNAP elements. The remodeled FT obstructs binding of RNA hairpins in the RNA exit tunnel next

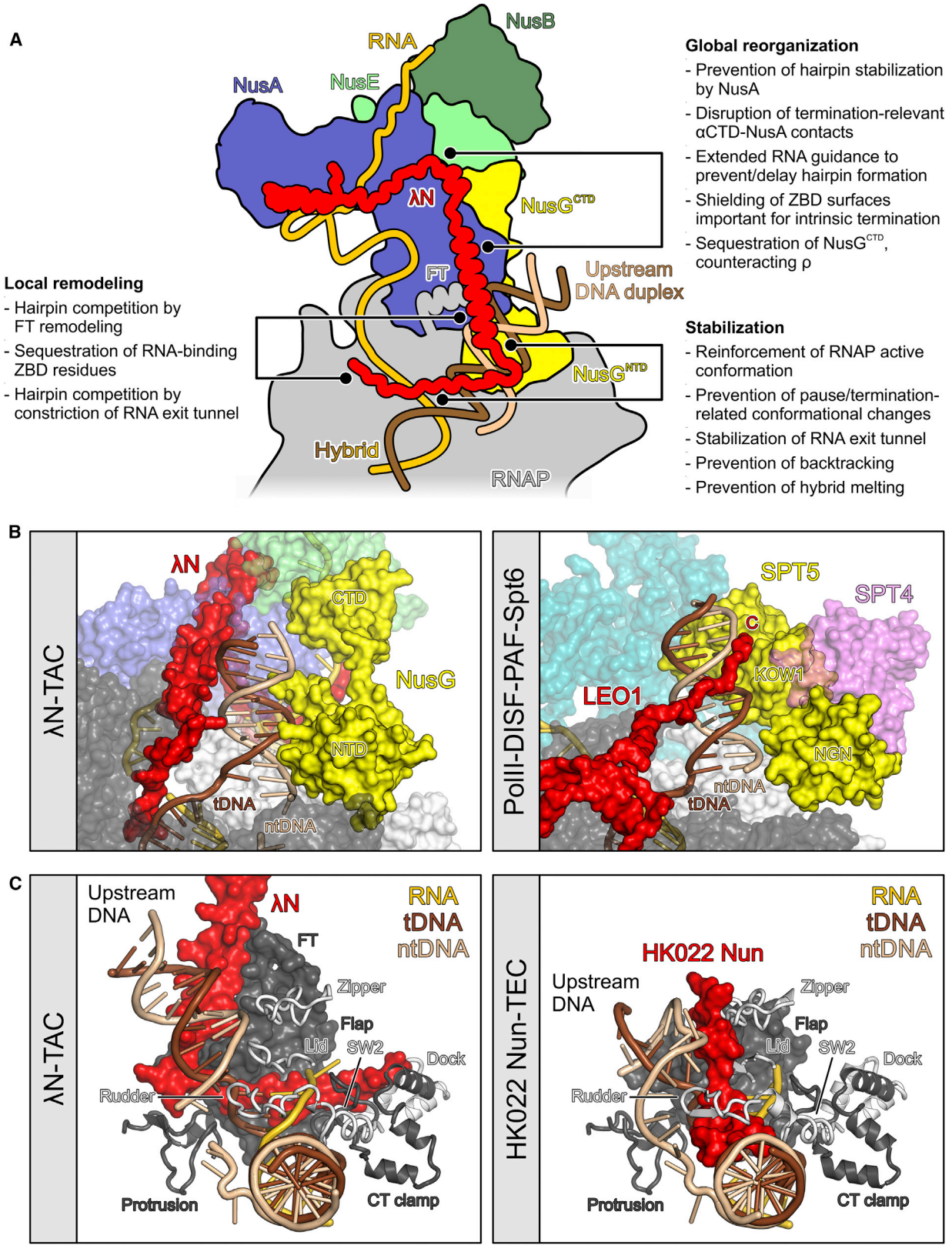

(legend on next page)

It can thereby bridge large distances and interact with the nascent RNA (*boxB*), upstream DNA, the hybrid, proteins of the regulatory RNP (NusA, NusE), and various elements of RNAP (FT, flap base, protrusion, CT clamp, and dock) that are remote from each other in the λN-TAC. Moreover, lack of a stable structure allows the C terminus to thread through the RNAP catalytic cavity.

Strategies to Maintain the Elongating Conformation

Pausing of multi-subunit RNAPs seems to be universally associated with a tilted 10-bp hybrid, with RNA in the post-translocated state and DNA in the pre-translocated state, that sequesters the +1 template base, as observed in *his*PECs (Guo et al., 2018; Kang et al., 2018a), a DRB sensitivity-inducing factor (DSIF)- and negative elongation factor (NELF)-paused Pol II TEC (Vos et al., 2018b), and an incompletely backtracked or slipped Pol II TEC (Cheung and Cramer, 2011). The tilted 10-bp hybrid is accommodated by small conformational changes in the flap, lid, clamp, and dock (Kang et al., 2018a), which can be further stabilized by transcription factor NusA in bacteria (Guo et al., 2018) or NELF in eukaryotes (Vos et al., 2018b). λN might favor an elongation-competent 9-bp hybrid and counteract transcriptional slippage (1) by contacting or running close to all the above RNAP elements, restricting their pausing-related movements, and (2) by capturing RNA immediately upstream of the hybrid. In addition, by binding the CT clamp, which in turn cradles the switch 2 region (β′ residues 330–349) that is thought to promote hybrid movement during translocation (Guo et al., 2018), λN might further stabilize a translocation-competent conformation.

Efficient rewinding of DNA immediately upstream of the hybrid stabilizes the post-translocated state in bacterial RNAP and eukaryotic Pol II (Klreeva et al., 2018). The eukaryotic NusG homolog SPT5, a subunit of DSIF, comprises a NusG-like NTD (NGN) and five NusG CTD-like KOW domains (KOW1–5). As in the λN-TAC, the SPT5 NGN binds across the active site cleft and abuts the upstream DNA in paused and activated Poll II TECs (Vos et al., 2018a; Vos et al., 2018b). Furthermore, KOW1 binds upstream DNA. In a DSIF/Pol II-Associated Factor 1(PAF1)- and SPT6-activated Poll II TEC (Vos et al., 2018a), the C-terminal extension of the PAF1 subunit LEO1 additionally lines upstream DNA similar to the central α3 helix of λN, albeit along a different surface (Figure 7B), suggesting similar strategies in supporting DNA rewinding and stabilization of an active conformation.

Regulation via the RNAP Inner Tunnel System

The λN C-terminal part represents a remarkable example of how a factor can take advantage of the system of RNAP channels, tunnels, and cavities for regulation. λN accesses the active site cavity on one side of the upstream DNA, where only minimal adjustments in RNAP elements are required to grant an unobstructed path across the hybrid to the RNA exit tunnel (Figure 7C). While positively charged λN side chains point toward upstream DNA, the hybrid and exiting RNA, these side chains are grouped in linear arrays, suggesting that nucleotides can be easily "handed over" from one to the next with the number and types of interactions maintained. Thus, λN seems to form a "non-stick" lateral surface for the nucleic acids, which still allows nucleic acid movement as required for RNA chain elongation. Recently, the cryo-EM structure of a HK022 Nun-stalled TEC showed how the C terminus of Nun can also access the active site cleft along a different flank of upstream DNA (Kang et al., 2017). Nun's C-terminal 23 residues fit snugly between the β′ zipper (β′ residues 36–61), lid, rudder (β′ residues 308–327), switch 2, upstream DNA, and the hybrid (Figure 7C), displacing several RNAP elements and upstream DNA. Notably, while λN runs alongside the nucleic acid scaffold, the C terminus of Nun is wedged in between the nucleic acids, preventing their movement and thus arresting RNAP. The different λN and Nun binding modes illustrate how opposite effects can be achieved by proteins entering RNAP through neighboring openings.

STAR★METHODS

Detailed methods are provided in the online version of this paper and include the following:

- KEY RESOURCES TABLE
- CONTACT FOR REAGENT AND RESOURCE SHARING
- EXPERIMENTAL MODEL AND SUBJECT DETAILS
- METHOD DETAILS
  - Sample Production
  - Cryo-EM Analysis of the λN-TAC
  - Analysis of Flexibility in the λN-TAC
  - Model Building and Refinement
  - Transcription Assays
- QUANTIFICATION AND STATISTICAL ANALYSIS
- DATA AND SOFTWARE AVAILABILITY

SUPPLEMENTAL INFORMATION

Supplemental Information includes four figures and two videos and can be found with this article online at https://doi.org/10.1016/j.molcel.2019.01.016.

ACKNOWLEDGMENTS

Synthetic $\lambda N^{88–107}$ peptide was a kind gift from Romina Schnegotzki and Roderich Süßmuth, Technische Universität Berlin. We acknowledge access to a 300 kV FEI Titan Krios transmission electron microscope at the European Molecular Biology Laboratory, Heidelberg, Germany, via iNEXT (http://www.inext-eu.org; PID 2231). We thank Wim Hagen and Carsten Sachse for help during cryo-EM data collection. We also acknowledge access to high-performance computing resources of the North German Supercomputing Alliance (HLRN) and support by Christian Tuma, Zuse Institut Berlin. Y.-H.H. was sponsored by a fellowship from the Chinese Scholarship Council. This work was supported by the Deutsche Forschungsgemeinschaft (SFB 740 to T.M., C.M.T.S., and M.C.W. and grant SFB 958 to M.C.W.).

Figure 7. Model Illustrating λN Action

(A) Summary of suggested mechanisms employed by λN to suppress transcriptional pausing and termination.

(B) Comparison of upstream DNA binding by λN (left) and LEO1 in a DSIF-PAF1-SPT6-activated Pol II TEC (PDB ID 6GMH).

(C) Comparison of λN and HK022 Nun (PDB ID 6ALG) entering the active site cleft.

AUTHOR CONTRIBUTIONS

F.K., N.S., Y.-H.H., B.L., and J.B. performed the experiments. T.M., C.M.T.S., and M.C.W. supervised the experiments. All authors contributed to the analysis of the data and the interpretation of the results. M.C.W. wrote the manuscript with contributions from the other authors.

DECLARATION OF INTERESTS

The authors declare no competing interests.

Received: July 23, 2018
Revised: December 4, 2018
Accepted: January 11, 2019
Published: February 19, 2019

SUPPORTING CITATIONS

The following reference appears in the Supplemental Information: Pettersen et al. (2004).

REFERENCES

Afonine, P.V., Grosse-Kunstleve, R.W., Echols, N., Headd, J.J., Moriarty, N.W., Mustyakimov, M., Terwilliger, T.C., Urzhumtsev, A., Zwart, P.H., and Adams, P.D. (2012). Towards automated crystallographic structure refinement with phenix.refine. Acta Crystallogr. D Biol. Crystallogr. *68*, 352–367.

Belogurov, G.A., and Artsimovitch, I. (2015). Regulation of transcript elongation. Annu. Rev. Microbiol. *69*, 49–69.

Burmann, B.M., Schweimer, K., Luo, X., Wahl, M.C., Stitt, B.L., Gottesman, M.E., and Rösch, P. (2010). A NusE:NusG complex links transcription and translation. Science *328*, 501–504.

Cheeran, A., Babu Suganthan, R., Swapna, G., Bandey, I., Achary, M.S., Nagarajaram, H.A., and Sen, R. (2005). Escherichia coli RNA polymerase mutations located near the upstream edge of an RNA:DNA hybrid and the beginning of the RNA-exit channel are defective for transcription antitermination by the N protein from lambdoid phage H-19B. J. Mol. Biol. *352*, 28–43.

Cheeran, A., Kolli, N.R., and Sen, R. (2007). The site of action of the antiterminator protein N from the lambdoid phage H-19B. J. Biol. Chem. *282*, 30997–31007.

Chen, V.B., Wedell, J.R., Wenger, R.K., Ulrich, E.L., and Markley, J.L. (2015). MolProbity for the masses-of data. J. Biomol. NMR *63*, 77–83.

Cheung, A.C., and Cramer, P. (2011). Structural basis of RNA polymerase II backtracking, arrest and reactivation. Nature *471*, 249–253.

Darst, S.A. (2001). Bacterial RNA polymerase. Curr. Opin. Struct. Biol. *11*, 155–162.

Emsley, P., and Cowtan, K. (2004). Coot: model-building tools for molecular graphics. Acta Crystallogr. D Biol. Crystallogr. *60*, 2126–2132.

Epshtein, V., Cardinale, C.J., Ruckenstein, A.E., Borukhov, S., and Nudler, E. (2007). An allosteric path to transcription termination. Mol. Cell *28*, 991–1001.

Gollnick, P., and Babitzke, P. (2002). Transcription attenuation. Biochim. Biophys. Acta *1577*, 240–250.

Guo, X., Myasnikov, A.G., Chen, J., Crucifix, C., Papai, G., Takacs, M., Schultz, P., and Weixlbaumer, A. (2018). Structural basis for NusA stabilized transcriptional pausing. Mol. Cell *69*, 816–827.e4.

Gusarov, I., and Nudler, E. (2001). Control of intrinsic transcription termination by N and NusA: the basic mechanisms. Cell *107*, 437–449.

Ha, K.S., Toulokhonov, I., Vassylyev, D.G., and Landick, R. (2010). The NusA N-terminal domain is necessary and sufficient for enhancement of transcriptional pausing via interaction with the RNA exit channel of RNA polymerase. J. Mol. Biol. *401*, 708–725.

Headd, J.J., Echols, N., Afonine, P.V., Grosse-Kunstleve, R.W., Chen, V.B., Moriarty, N.W., Richardson, D.C., Richardson, J.S., and Adams, P.D. (2012). Use of knowledge-based restraints in phenix.refine to improve macromolecular refinement at low resolution. Acta Crystallogr. D Biol. Crystallogr. *68*, 381–390.

Herbert, K.M., Zhou, J., Mooney, R.A., Porta, A.L., Landick, R., and Block, S.M. (2010). E. coli NusG inhibits backtracking and accelerates pause-free transcription by promoting forward translocation of RNA polymerase. J. Mol. Biol. *399*, 17–30.

Hohn, M., Tang, G., Goodyear, G., Baldwin, P.R., Huang, Z., Penczek, P.A., Yang, C., Glaeser, R.M., Adams, P.D., and Ludtke, S.J. (2007). SPARX, a new environment for Cryo-EM image processing. J. Struct. Biol. *157*, 47–55.

Kang, J.Y., Olinares, P.D., Chen, J., Campbell, E.A., Mustaev, A., Chait, B.T., Gottesman, M.E., and Darst, S.A. (2017). Structural basis of transcription arrest by coliphage HK022 Nun in an *Escherichia coli* RNA polymerase elongation complex. eLife *6*, e25478.

Kang, J.Y., Mishanina, T.V., Bellecourt, M.J., Mooney, R.A., Darst, S.A., and Landick, R. (2018a). RNA polymerase accommodates a pause RNA hairpin by global conformational rearrangements that prolong pausing. Mol. Cell *69*, 802–815.e1.

Kang, J.Y., Mooney, R.A., Nedialkov, Y., Saba, J., Mishanina, T.V., Artsimovitch, I., Landick, R., and Darst, S.A. (2018b). Structural basis for transcript elongation control by NusG family universal regulators. Cell *173*, 1650–1662.

King, R.A., Banik-Maiti, S., Jin, D.J., and Weisberg, R.A. (1996). Transcripts that increase the processivity and elongation rate of RNA polymerase. Cell *87*, 893–903.

King, R.A., Markov, D., Sen, R., Severinov, K., and Weisberg, R.A. (2004). A conserved zinc binding domain in the largest subunit of DNA-dependent RNA polymerase modulates intrinsic transcription termination and antitermination but does not stabilize the elongation complex. J. Mol. Biol. *342*, 1143–1154.

Kireeva, M., Trang, C., Matevosyan, G., Turek-Herman, J., Chasov, V., Lubkowska, L., and Kashlev, M. (2018). RNA-DNA and DNA-DNA base-pairing at the upstream edge of the transcription bubble regulate translocation of RNA polymerase and transcription rate. Nucleic Acids Res. *46*, 5764–5775.

Kolb, K.E., Hein, P.P., and Landick, R. (2014). Antisense oligonucleotide-stimulated transcriptional pausing reveals RNA exit channel specificity of RNA polymerase and mechanistic contributions of NusA and RfaH. J. Biol. Chem. *289*, 1151–1163.

Lawson, M.R., Ma, W., Bellecourt, M.J., Artsimovitch, I., Martin, A., Landick, R., Schulten, K., and Berger, J.M. (2018). Mechanism for the regulated control of bacterial transcription termination by a universal adaptor protein. Mol. Cell *71*, 911–922.

Liu, K., Zhang, Y., Severinov, K., Das, A., and Hanna, M.M. (1996). Role of Escherichia coli RNA polymerase alpha subunit in modulation of pausing, termination and anti-termination by the transcription elongation factor NusA. EMBO J. *15*, 150–161.

Loerke, J., Giesebrecht, J., and Spahn, C.M. (2010). Multiparticle cryo-EM of ribosomes. Methods Enzymol. *483*, 161–177.

Luo, X., Hsiao, H.H., Bubunenko, M., Weber, G., Court, D.L., Gottesman, M.E., Urlaub, H., and Wahl, M.C. (2008). Structural and functional analysis of the *E. coli* NusB-S10 transcription antitermination complex. Mol. Cell *32*, 791–802.

Mah, T.F., Li, J., Davidson, A.R., and Greenblatt, J. (1999). Functional importance of regions in Escherichia coli elongation factor NusA that interact with RNA polymerase, the bacteriophage lambda N protein and RNA. Mol. Microbiol. *34*, 523–537.

Mason, S.W., Li, J., and Greenblatt, J. (1992). Host factor requirements for processive antitermination of transcription and suppression of pausing by the N protein of bacteriophage lambda. J. Biol. Chem. *267*, 19418–19426.

Mastronarde, D.N. (2005). Automated electron microscope tomography using robust prediction of specimen movements. J. Struct. Biol. *152*, 36–51.

Mooney, R.A., Schweimer, K., Rösch, P., Gottesman, M., and Landick, R. (2009). Two structurally independent domains of E. coli NusG create regulatory plasticity via distinct interactions with RNA polymerase and regulators. J. Mol. Biol. *391*, 341–358.

Moriya, T., Saur, M., Stabrin, M., Merino, F., Voicu, H., Huang, Z., Penczek, P.A., Raunser, S., and Gatsogiannis, C. (2017). High-resolution single particle analysis from electron cryo-microscopy images using SPHIRE. J. Vis. Exp. *123*, e55448.

Nudler, E., and Gottesman, M.E. (2002). Transcription termination and anti-termination in E. coli. Genes Cells *7*, 755–768.

Parks, A.R., Court, C., Lubkowska, L., Jin, D.J., Kashlev, M., and Court, D.L. (2014). Bacteriophage λ N protein inhibits transcription slippage by Escherichia coli RNA polymerase. Nucleic Acids Res. *42*, 5823–5829.

Penczek, P.A., Frank, J., and Spahn, C.M. (2006). A method of focused classification, based on the bootstrap 3D variance analysis, and its application to EF-G-dependent translocation. J. Struct. Biol. *154*, 184–194.

Pettersen, E.F., Goddard, T.D., Huang, C.C., Couch, G.S., Greenblatt, D.M., Meng, E.C., and Ferrin, T.E. (2004). UCSF Chimera—a visualization system for exploratory research and analysis. J. Comput. Chem. *25*, 1605–1612.

Ray-Soni, A., Bellecourt, M.J., and Landick, R. (2016). Mechanisms of bacterial transcription termination: all good things must end. Annu. Rev. Biochem. *85*, 319–347.

Roberts, J.W. (1969). Termination factor for RNA synthesis. Nature *224*, 1168–1174.

Rohou, A., and Grigorieff, N. (2015). CTFFIND4: Fast and accurate defocus estimation from electron micrographs. J. Struct. Biol. *192*, 216–221.

Said, N., Krupp, F., Anedchenko, E., Santos, K.F., Dybkov, O., Huang, Y.H., Lee, C.T., Loll, B., Behrmann, E., Bürger, J., et al. (2017). Structural basis for λN-dependent processive transcription antitermination. Nat. Microbiol. *2*, 17062.

Scheres, S.H. (2015). Semi-automated selection of cryo-EM particles in RELION-1.3. J. Struct. Biol. *189*, 114–122.

Shankar, S., Hatoum, A., and Roberts, J.W. (2007). A transcription antiterminator constructs a NusA-dependent shield to the emerging transcript. Mol. Cell *27*, 914–927.

Sherwood, A.V., and Henkin, T.M. (2016). Riboswitch-mediated gene regulation: novel RNA architectures dictate gene expression responses. Annu. Rev. Microbiol. *70*, 361–374.

Svetlov, V., and Artsimovitch, I. (2015). Purification of bacterial RNA polymerase: tools and protocols. Methods Mol. Biol. *1276*, 13–29.

Tang, G., Peng, L., Baldwin, P.R., Mann, D.S., Jiang, W., Rees, I., and Ludtke, S.J. (2007). EMAN2: an extensible image processing suite for electron microscopy. J. Struct. Biol. *157*, 38–46.

Toulokhonov, I., and Landick, R. (2003). The flap domain is required for pause RNA hairpin inhibition of catalysis by RNA polymerase and can modulate intrinsic termination. Mol. Cell *12*, 1125–1136.

Toulokhonov, I., Artsimovitch, I., and Landick, R. (2001). Allosteric control of RNA polymerase by a site that contacts nascent RNA hairpins. Science *292*, 730–733.

Turtola, M., and Belogurov, G.A. (2016). NusG inhibits RNA polymerase backtracking by stabilizing the minimal transcription bubble. eLife *5*, e18096.

Van Gilst, M.R., and von Hippel, P.H. (1997). Assembly of the N-dependent antitermination complex of phage lambda: NusA and RNA bind independently to different unfolded domains of the N protein. J. Mol. Biol. *274*, 160–173.

Vos, S.M., Farnung, L., Boehning, M., Wigge, C., Linden, A., Urlaub, H., and Cramer, P. (2018a). Structure of activated transcription complex Pol II-DSIF-PAF-SPT6. Nature *560*, 607–612.

Vos, S.M., Farnung, L., Urlaub, H., and Cramer, P. (2018b). Structure of paused transcription complex Pol II-DSIF-NELF. Nature *560*, 601–606.

Weisberg, R.A., and Gottesman, M.E. (1999). Processive antitermination. J. Bacteriol. *181*, 359–367.

Zhang, J., and Landick, R. (2016). A two-way street: regulatory interplay between RNA polymerase and nascent RNA structure. Trends Biochem. Sci. *41*, 293–310.

Zheng, S.Q., Palovcak, E., Armache, J.P., Verba, K.A., Cheng, Y., and Agard, D.A. (2017). MotionCor2: anisotropic correction of beam-induced motion for improved cryo-electron microscopy. Nat. Methods *14*, 331–332.

STAR★METHODS

KEY RESOURCES TABLE

REAGENT or RESOURCE	SOURCE	IDENTIFIER
Bacterial and Virus Strains		
Escherichia coli Rosetta2 DE3	Novagen	Cat No. 70954-3
Chemicals, Peptides, and Recombinant Proteins		
pVS10 (*E. coli* RNAP co-expression plasmid for α-, β-, C-terminally His_6-tagged β'-, and ω-subunits)	Svetlov and Artsimovitch, 2015	N/A
pIA1159 (*E. coli* RNAP co-expression plasmid for C-terminally His_6-tagged α [Δ235-end] -, β-, β'-, and ω-subunits)	Svetlov and Artsimovitch, 2015	N/A
pETM11-NusA (*E. coli* NusA full-length, deletion and mutation proteins with cleavable N-terminal $(His)_6$-tag)	Said et al., 2017 and this study	N/A
pETM11-NusB (*E. coli* NusB protein with cleavable N-terminal $(His)_6$-tag)	Luo et al., 2008	N/A
pGEX-6p1-NusG (*E. coli* NusG protein with cleavable N-terminal GST-tag)	Said et al., 2017 and this study	N/A
pGEX-6p1-NusE (*E. coli* NusE protein with cleavable N-terminal GST-tag)	Luo et al., 2008	N/A
pGEX-6p1-λN (Bacteriophage λ N full-length, deletion and mutation proteins with cleavable N-terminal GST-tag)	Said et al., 2017 and this study	N/A
pETM-11-Rho	This study	N/A
$λN^{88-107}$ peptide	Roderich Süßmuth, TU Berlin, Germany	N/A
Deposited Data		
E. coli RNAP-NusA-NusG-NusB-NusE-λN	This paper	PDB: 6GOV
RNAP-NusA-NusG-NusB-NusE-λN cryo-EM maps	This paper	EMDB: EMD-0043
Original gel images	This paper	https://doi.org/10.17632/tp4n84ny5g.1
Experimental Models: Organisms/Strains		
Escherichia coli	N/A	N/A
Oligonucleotides		
Template DNA, DNAIIb (tDNA): CTTGTTATCCGCTCA CAATGCCACACGCCTAACGAGCCGGAAGCATAAA GTGTAAAGCCTTTTTT	Said et al., 2017	N/A
Non-template DNA, DNAI (ntDNA): AAAAAAGGCTTT ACACTTTATGCTTCCGGCTCGTATAATCGCACCTTA TGTGAGCGGATAACAAG	Said et al., 2017	N/A
nut RNA: GGCGCUCUUUAACAUUAAGCCCUGAAG AAGGGCAAAAAUCAAAUUAAACCACACCUGGCG UGUGGC	Said et al., 2017	N/A

(*Continued on next page*)

Continued

REAGENT or RESOURCE	SOURCE	IDENTIFIER
pNS-31- DNA template for transcription assay (includes *nut* site): AAGCTTTCAGATCTCTCACCTAC CAAACAATGCCCCCCTGCAAAAAATAAATTCATAT AAAAAACATACAGATAACCATCTGCGGTGATAAAT TATCTCTGGCGGTGTTGACATAAATACCACTGGC GGTGATACTGAGCACATCAGCAGGACGCACTGA CCACCATGAAGGTGACGCTCTTAAAAATTAAGCC CTGAAGAAGGGCAGCATTCAAAGCAGAAGGCTT TGGGGTGTGTGATACGAAACGAAGCATTGGCCG TAAGTGCGATTCCGGATTAGCTGCCAATTCTAGC ATGCCTGCAGGTCGACTCTAGATCAGATCTCTCA CCTACCAAACAAGGGAAAATCGATTCCTCTTATC TAGCGCGGGGGGTTTTCAATCCCGAAACAGTTC GCAGGTAATAGTTAGAGCCTGCATAACGGTTTC GGGATTTTTTCGCGGCATAACATGCAGTGGACGC CAGAAAATTAAGGGAAAATCGATTCCTCTTATCTAG ggtaccgagctcgaattcgtaatcatggtcatagctgtttcctgtgtga aattgttatccgctcacaatt ccacacaacatacgagccggaagca taaagtgtaaagcctggggtgcctaatgagtgagctaactcacatta attgcgttgcg	Said et al., 2017	N/A
pNS-33 - DNA template for transcription assay (includes shortened distance between *nut* side and tR'): AAGCTTTCAGATCTCTCACCTACCAAACAATGCCCC CCTGCAAAAAATAAATTCATATAAAAAACATACAGA TAACCATCTGCGGTGATAAATTATCTCTGGCGGTGT TGACATAAATACCACTGGCGGTGATACTGAGCACATC AGCAGGACGCACTGACCACCATGAAGGTGACGCTC TTAAAAATTAAGCCCTGAAGAAGGGCAGCTCTAGATC AGATCTCTCACCTACCAAACAAGGGAAAATCGATTCC TCTTATCTAGCGCGGGGGGTTTTCAATCCCGAAACAG TTCGCAGGTAATAGTTAGAGCCTGCATAACGGTTTCG GGATTTTTTCGCGGCATAACATGCAGTGGACGCCAGA AAATTAAGGGAAAATCGATTCCTCTTATCTAGgtaccga gctcgaattcgtaatcatggt catagctgtttcctgtgtgaaattgttatccgc tcacaattccacacaacatacgagccggaagcataaagtgtaaagcctgg ggtgcctaatgagtgagctaactcacattaattgcgttgcg	This study	N/A
pNS-34 - DNA template for transcription assay with Rho-dependent terminator (includes *nut* and *rut* side): AAGCTA ATTATAATTATAATTATAATTATAATTATCTCTGGCGGTGTT GACTTAAAGTCTAACCTATAGTATAATTACAGCCATCGAGAG GGACACGGGGAAACACCACCAATAACCCCGCTCTTACACA TTCCAGCCCTGAAAAAGGGCATCAAATTAAACCACACCTAT GGTGTATGCATTTATTTGCATACATTCAATCAATTGTTATCTA AGGAAATACTTACATATGGTTCGTGCTCTAGATCAGATCTCT CACCTACCAAACAAGGGAAAATCGATTCCTCTTATCTAGCG CGGGGGGTTTTCAATCCCGAAACAGTTCGCAGGTAATAGTT AGAGCCTGCATAACGGTTTCGGGATTTTTTCGCGGCATAAC ATGCAGTGGACGCCAGAAAATTAAGGGAAAATCGATTCCTC TTATCTAGGGTACCGAGCTCGAATTCGTAATCATGGTCATAG CTGTTTCCTGTGTGAAATTGTTATCCGCTCACAATTCCACAC AACATACGAGCCGGAAGCATAAAGTGTAAAGCCTGGGGTGC CTAATGAGTGAGCTAACTCACATTAATTGCGTTGCG	This study	N/A
Software and Algorithms		
CTFFind4	Rohou and Grigorieff, 2015	https://grigoriefflab.janelia.org/ctffind4
Motioncor2	Zheng et al., 2017	http://msg.ucsf.edu/em/software/motioncor2.html
EMAN v2.2	Tang et al., 2007	https://blake.bcm.edu/emanwiki/EMAN2

(*Continued on next page*)

Continued

REAGENT or RESOURCE	SOURCE	IDENTIFIER
Relion 1.3	Scheres, 2015	https://www2.mrc-lmb.cam.ac.uk/relion/index.php?title=Main_Page
SPHIRE	Moriya et al., 2017	http://sphire.mpg.de/
SPARX	Hohn et al., 2007	http://sparx-em.org/sparxwiki/
COOT v0.8.3	Emsley and Cowtan, 2004	https://www2.mrc-lmb.cam.ac.uk/personal/pemsley/coot/
PHENIX	Afonine et al., 2012	https://www.phenix-online.org

CONTACT FOR REAGENT AND RESOURCE SHARING

Further information and request for resources and reagents should be directed to and will be fulfilled by the Lead Contact, Markus C. Wahl (markus.wahl@fu-berlin.de).

EXPERIMENTAL MODEL AND SUBJECT DETAILS

For plasmid construction, we used the *Escherichia coli* (*E. coli*) DH5α strain (Thermo Fisher Scientific). For recombinant protein expression we used *E. coli* Rosetta2 DE3 (Novagen).

METHOD DETAILS

Sample Production

DNA, RNA and protein components of the λN-TAC and variants thereof were produced and purified as described before (Said et al., 2017). λN and NusA point mutations were introduced by site-directed mutagenesis using the QuikChange protocol (Stratagene). For N-terminally truncated λN variants (residues 38-107, 58-107), C-terminally truncated λN variants (residues 1-62, 1-84, 1-90, 1-99, 1-104) and a NusA truncation variant containing only the NTD and NTD-S1 linker helix (residues 1-137), the corresponding DNA fragments were PCR-amplified from plasmids encoding the full-length proteins and cloned into pGEX-6P-1 (λN constructs) or pETM-11 (NusA construct) as described (Said et al., 2017). All expression constructs were verified by DNA sequencing (Seqlab). Protein variants were produced and purified using the same protocols as for the wild-type proteins (Said et al., 2017). A synthetic, HPLC-purified peptide comprising the λN C terminus (λN^{88-107}) was obtained from the group of Roderich Süßmuth, Technische Universität Berlin.

A DNA fragment encoding the NusG NTD (residues 1-116) was amplified from a plasmid containing the full-length NusG coding region and cloned into pGEX-6P-1. $NusG^{NTD}$ was purified as the wild-type NusG (Said et al., 2017). DNA encoding ρ was cloned into pETM-11, removing a vector-contained region coding for an N-terminal His_6-tag, and expressed in *E. coli* Rosetta (DE3) cells (Novagen). Cells were lysed in 50 mM Tris-HCl, pH 7.5, 50 mM KCl, 1mM DTT, 10% (v/v) glycerol. Cleared lysate was loaded on a 5 mL Heparin Sepharose column (GE Healthcare) in buffer A (50 mM Tris-HCl, pH 7.5, 50 mM NaCl, 1 mM DTT) and eluted with buffer A plus 1 M NaCl. Peak fractions were pooled and further purified by gel filtration chromatography in 10 mM Tris-HCl, pH 7.5, 50 mM NaCl, 1 mM DTT.

Cryo-EM Analysis of the λN-TAC

For λN-TAC formation, equimolar amounts of non-template DNA, template DNA and *nut* RNA were mixed in reaction buffer (20 mM HEPES-NaOH, pH 7.5, 50 mM NaCl, 5 mM $MgCl_2$, 1 mM DTT) and annealed by heating to 95°C for 5 min and subsequent cooling to 10°C at 1°C/min to generate an annealed scaffold (Figure 1A). The annealing product was then incubated with RNAP in a 1:0.8 molar ratio on ice for 10 min, then at room temperature for 15 min. Afterward, a 1.2-fold molar excess of NusA/B/E/G and λN protein was added, followed by incubation at room temperature for 15 min. The mixture was subsequently applied to a Superdex 200 Increase 3.2/300 column (GE Healthcare) and fractions of the complex were pooled. Purified complex (0.3 mg/mL) was flash frozen on Quantifoil R2/4 grids covered with an additional carbon layer, using a Vitrobot plunger (FEI) with 2-4 s blotting time and the blotting chamber at 4°C and 100% humidity (Said et al., 2017).

Grids were screened for initial data collection using a 120 kV Tecnai G2 Spirit TEM (FEI) equipped with a F416 CMOS camera (TVIPS). For high-resolution cryo-EM reconstruction, micrographs were acquired on a Titan Krios transmission electron microscope (FEI), operated at 300 kV, using a GIF energy filter and a K2 direct electron detector (Gatan), operated in super-resolution mode (European Molecular Biology Laboratory, Heidelberg). Automated data collection was performed using SerialEM (Mastronarde, 2005) and an in-house script (Wim Hagen, European Molecular Biology Laboratory, Heidelberg) for target selection. In total, 4,074 video stacks (40 frames with 20 s total exposure time, dose rate of 3.45 $e/Å^2/s$ and beam diameter of 800 nm) were acquired at 105.000x magnification resulting in a pixel size of 0.675 Å/pixel at the object scale, using a 50 μm C2 aperture, a 70 μm objective aperture and a defocus range of 0.75-3.3 μm in a uniform distribution.

Initial CTF parameters were estimated using CTFFind4 (Rohou and Grigorieff, 2015). Frame alignment, gain correction and dose-weighting were performed with MotionCorr2 (Zheng et al., 2017), using the following parameters: 5x5 patches, 10 iterations, Fm dose 1.75e/A^2/frame, Tol 0.5, frames 1-40. Aligned micrographs and results from CTFFind4 were visually inspected. 3,550 micrographs were selected for further processing. 802,858 particle images were picked using EMAN2 (Tang et al., 2007) with e2boxer.py operated in "swarm" mode. Box coordinates were scaled up appropriately and used for particle extraction at 6-fold decimation (4.05 Å/pixel) with Relion 1.3 (Scheres, 2015). 2D classification was performed in 25 iterations using Relion 1.3 with the following parameters: psi_step 20.0, offset_range 6, offset_step 4, strict_highres_exp 12, oversampling 1, particle diameter 260 Å, tau2_fudge 2, classes K 100, zero_mask true, dont_check_norm. 708,030 particle images were selected for further refinement by visual inspection of the 2D class averages (Figure S1B). The particles were re-extracted at 2-fold decimation (1.35 Å/pixel) using SPHIRE (Moriya et al., 2017) and refined to high-resolution using sxmeridien.py with the following parameters: radius 110 px, initial resolution 15 Å, search range 5 px, translation step 1 px. Two unfiltered half maps were combined and sharpened using a B-factor of −97 A^2, yielding resolutions of 3.95 Å and 3.68 Å at the FSC-criteria 0.5 and 0.143, respectively (Figure S2A,B). Local resolution was calculated using sxlocres.py with a soft mask based on the sharpened map, FSC window size 7 px and a radius 110 px. The resulting mask indicated regions of different resolution and was used for local filtration via sxfilterlocal.py (Figure S2C).

Analysis of Flexibility in the λN-TAC

Lower resolution of the cryo-EM map around the bulk of the λN-NusA-NusB-NusE-*nut* RNA complex indicated a high degree of flexibility of this element relative to RNAP. 3D variability was calculated using a radius of 110 px and 10 images per group (Moriya et al., 2017). The resulting density map was filtered to define the structurally heterogeneous area. A binary mask was created based on this variability map and used for focused classification (Penczek et al., 2006). Focused classification only considered information within the binary mask and was carried out by an incremental K-means-like method of unsupervised 3D sorting (Loerke et al., 2010) implemented using SPARX (Hohn et al., 2007). RNAP alone was added as a neutral reference every 4-6 iterations. 32 iterations separated the dataset into 7 classes (Tier 1; Figure S3A). Particle images from four classes (409,679 particle images) could be further separated into 8 classes (Tier 2). The largest classes were refined individually to resolutions of 4.8 Å, 4.2 Å and 4.4 Å, respectively (Maps 2, 3 and 4; Figure S3), representing different states of the modifying RNP. Further refinement of other classes did not result in interpretable high-resolution maps for the modifying RNP region (Figure S3A).

Model Building and Refinement

The final, globally B-factor sharpened, locally filtered cryo-EM map was used for model building. Coordinates of an *E. coli* TEC (PDB ID 6ALH), of a λN-NusA-NusB-NusE-*nut* RNA complex (PDB ID 5LM7) and of NusG N- and C-terminal domains (PDB IDs 2K06 and 2JVV) were docked into the cryo-EM map using COOT (Emsley and Cowtan, 2004). Portions connecting the λN-NusA-NusB-NusE-*nut* RNA complex and RNAP (NusA NTD, λN central α-helix), the FT, the λN C terminus and the nucleic acids were manually rebuilt into the cryo-EM density. The entire structure was manually adjusted residue-by-residue, supported by real space refinement in COOT. The manually built model was refined against the cryo-EM map using the real space refinement protocol in PHENIX (Afonine et al., 2012). Initial refinement was locally restrained by using partial models as references (RNAP – PDB ID 5LM7; modifying RNP – PDB ID 6ALH; NusA – PDB ID 5LM9, NusB – PDB ID 3D3B, λN – PDB ID 3D3B, NusG NTD – PDB ID 2K06, NusG CTD – PDB ID 2JVV; (Headd et al., 2012). These restraints were omitted in later refinement steps.

Transcription Assays

Single-round transcription anti-termination assays were performed as described (Said et al., 2017) and analyzed by denaturing (6 M urea) polyacylamide gel electrophoresis (PAGE; 8%). To test functionality of *in vitro* assembled λN-TAC, λN-TAC (or a λN-TAC with λN$^{1-84}$ or an otherwise identical TEC lacking λN) at 50 nM concention was mixed with 1 μCi [α-^{32}P] ATP in 10 mM Tris-HCl, pH 7.9, 10 mM $MgCl_2$, 100 mM KCl, 1 mM DTT (10 μl final volume), incubated at 32°C for 10 min and then incubated on ice for 5 min. To start run-off transcription, 1 μl of an ice-cold 1 mM solution of all four NTPs was added to the reaction mix on ice. Reactions were stopped at selected time points by mixing with 10% SDS. RNAs were PCI-extracted, precipitated by isopropanol and separated by denaturing PAGE (10%). RNA bands were visualized using a Storm phospohorimager and quantified using Image-Quant software (GE Healthcare). Data were analyzed by plotting the fraction of run-off transcript versus time and fitting the data to a first-order reaction (fraction $RO = A[1\text{-}\exp(-k_e\, t)]$; *RO*, run-off transcript; *A,* amplitude of the reaction; k_e, apparent first-order rate constant of transcription elongation; t, time).

To test the effects of some truncated λN variants, assays were performed with a DNA template that contained the same elements as above but with a shorter distance between the *nut* site and *λtR'* (73 nts compared to 174 nts in the longer version). A TEC was assembled as described (Said et al., 2017), which was subsequently incubated with 500 nM λN or λN variants at 32°C for 10 min. RNA chain elongation was started by adding pre-heated NTPs to final concentrations of 2 mM (ATP) or 50 μM (UTP, GTP and CTP). Reactions were stopped after 15 min, followed by RNA extraction, analysis by denaturing PAGE (8%) and visualization and quantification as described above. Control experiments were conducted with RNAP alone.

For *in vitro* transcription assays with ρ, a DNA template was used, which contained the *T7A1* promoter followed by a 158-bp element derived from a sequence immediately downstream of the *cro* gene of phage λ. The latter segment contains the *nut* and *rut* sites of the *λtR1* terminator and the remainder of the terminator region. This sequence is followed by the *λtR'* intrinsic

terminator. ρ was added to a final concentration of 500 nM hexamer where indicated and assays were performed as described (Said et al., 2017).

QUANTIFICATION AND STATISTICAL ANALYSIS

At least three independent experiments were performed for each analysis that was statistically analyzed. Significance was assessed by Student's unpaired t test; significance indicators: * - $p < 0.05$; ** - $p < 0.01$; *** - $p < 0.001$; ns - not significant ($p \geq 0.05$).

DATA AND SOFTWARE AVAILABILITY

Structure coordinates for the λN-TAC were deposited with the Protein Data Bank under accession code 6GOV. Cryo-EM maps for the λN-TAC were deposited with the Electron Microscopy Data Bank under accession code EMD-0043. Original gel images are available at: https://doi.org/10.17632/tp4n84ny5g.1